Frequency characteristics of dissipative and generative fractional RLC circuits

Kristian Haška
Dušan Zorica
Stevan Cvetićanin (stevan.cveticanin@uns.ac.rs)

Research Article

Keywords: dissipative and generative capacitor and inductor, fractional series RLC circuits, frequency characteristics of transfer function modulus and argument

Posted Date: October 21st, 2021

DOI: https://doi.org/10.21203/rs.3.rs-1003651/v1

Version of Record: A version of this preprint was published at Circuits, Systems, and Signal Processing on April 18th, 2022. See the published version at https://doi.org/10.1007/s00034-022-02025-3.

Frequency characteristics of dissipative and generative fractional RLC circuits

Kristian Haška* Dušan Zorica†‡ Stevan M. Cvetićanin§

October 21, 2021

Abstract

Equations governing the transient and steady-state regimes of the fractional series RLC circuits containing dissipative and/or generative capacitor and inductor are posed by considering the electric current as a response to electromotive force. Further, fractional RLC circuits are analyzed in the steady-state regime and their energy consumption/production properties are established depending on the angular frequency of electromotive force. Frequency characteristics of the modulus and argument of transfer function, i.e., of circuit's equivalent admittance, are analyzed through the Bode diagrams for the whole frequency range, as well as for low and high frequencies as the asymptotic expansions of transfer function modulus and argument.

Key words: dissipative and generative capacitor and inductor, fractional series RLC circuits, frequency characteristics of transfer function modulus and argument

1 Introduction

Electric elements made of materials having history dependent polarization and magnetization processes rather than only instantaneous ones, can be constitutively modeled by adding a hereditary type term in a classical constitutive equation, as proposed in [14], so that in the case of capacitor one may express either charge q at the time-instant $t > 0$ in terms of history of capacitor voltage u_C, or vice versa, as

$$q(t) = C\,u_C(t) + C_\alpha\,{}_0\mathrm{I}_t^{1-\alpha} u_C(t), \quad \alpha \in (0,1), \tag{1}$$

$$u_C(t) = \frac{1}{C}\,q(t) + \frac{1}{C_\mu}\,{}_0\mathrm{I}_t^{\mu} q(t), \quad \mu \in (0,1), \tag{2}$$

where ${}_0\mathrm{I}_t^{\xi}$ denotes the Riemann-Liouville fractional integral of order $\xi > 0$, defined as in [23] by

$${}_0\mathrm{I}_t^{\xi} f\,(t) = \frac{t^{\xi-1}}{\Gamma\,(\xi)} * f\,(t) = \frac{1}{\Gamma(\xi)} \int_0^t \frac{f(t')}{(t-t')^{1-\xi}}\mathrm{d}t',$$

where Γ is the Euler gamma function, with $*$ denoting the convolution and $C[\mathrm{F}]$, $C_\alpha[\frac{\mathrm{F}}{\mathrm{s}^{1-\alpha}}]$, and $C_\mu[\mathrm{F\,s}^\mu]$ being classical and fractional capacitances, while for the inductor, the same type of equations express either magnetic flux ϕ in terms of history of inductor current i_L, or vice versa, reading

$$\phi(t) = L\,i_L(t) + L_\beta\,{}_0\mathrm{I}_t^{1-\beta} i_L(t), \quad \beta \in (0,1), \tag{3}$$

$$i_L(t) = \frac{1}{L}\,\phi(t) + \frac{1}{L_\nu}\,{}_0\mathrm{I}_t^{\nu} \phi(t), \quad \nu \in (0,1), \tag{4}$$

where $L[\mathrm{H}]$, $L_\beta[\frac{\mathrm{H}}{\mathrm{s}^{1-\beta}}]$, and $L_\nu[\mathrm{H\,s}^\nu]$ are classical and fractional inductances. Although constitutive models (1) - (4) share the same mathematical form, they describe different elements regarding the energy

*Department of Power, Electronic and Telecommunication Engineering, Faculty of Technical Sciences, University of Novi Sad, Trg D. Obradovića 6, 21000 Novi Sad, Serbia, kristian.haska@uns.ac.rs

†Department of Physics, Faculty of Sciences, University of Novi Sad, Trg D. Obradovića 4, 21000 Novi Sad, Serbia, dusan.zorica@df.uns.ac.rs

‡Mathematical Institute, Serbian Academy of Arts and Sciences, Kneza Mihaila 36, 11000 Beograd, Serbia, dusan_zorica@mi.sanu.ac.rs

§Department of Power, Electronic and Telecommunication Engineering, Faculty of Technical Sciences, University of Novi Sad, Trg D. Obradovića 6, 21000 Novi Sad, Serbia, stevan.cveticanin@uns.ac.rs

consumption and production properties, since models (1) and (3) correspond to the dissipative capacitor and inductor, while models (2) and (4) represent elements' generative counterparts, according to the thermodynamic analysis of elements' steady state regime conducted in [14]. Fractional electric elements modeled by (2) and (3) can be viewed as a series connection of either classical and generative fractional capacitor, or classical and dissipative fractional inductor, while models (1) and (4) represent a parallel connection of either classical and dissipative fractional capacitor, or classical and generative fractional inductor.

The aim is to analyze thermodynamic properties and frequency characteristics of the fractional RLC circuit formed by the series connection of dissipative capacitor and inductor, modeled by (1) and (3), already considered in [15] in transient and steady state regimes, along with three other combinations of dissipative/generative capacitor and inductor forming series RLC circuits. Governing equation corresponding to the dissipative-dissipative RLC circuit, formed as a series connection of resistor with dissipative capacitor and inductor, is obtained in Section 2 as

$$R\bigg(\tau_L\tau_C\,\frac{\mathrm{d}^2}{\mathrm{d}t^2}+\tau_L\tau_\alpha\,{}_0\mathrm{D}_t^{1+\alpha}+\tau_C\tau_\beta\,{}_0\mathrm{D}_t^{1+\beta}+\tau_\alpha\tau_\beta\,{}_0\mathrm{D}_t^{\alpha+\beta}+\tau_C\,\frac{\mathrm{d}}{\mathrm{d}t}+\tau_\alpha\,{}_0\mathrm{D}_t^{\alpha}+1\bigg)i(t)=\bigg(\tau_C\frac{\mathrm{d}}{\mathrm{d}t}+\tau_\alpha\,{}_0\mathrm{D}_t^{\alpha}\bigg)\mathcal{E}(t), \tag{5}$$

by coupling constitutive equations (1) and (3) with the second Kirchhoff's and Ohm's laws. Analogously, using constitutive equations of generative capacitor and inductor (2) and (4), equation

$$R\bigg(\tau_\nu\,{}_0\mathrm{D}_t^{1+\nu}+\frac{\tau_\nu}{\tau_L}\,{}_0\mathrm{D}_t^{\nu}+1+\frac{\tau_\nu}{\tau_L\tau_C}\,{}_0\mathrm{I}_t^{1-\nu}+\frac{1}{\tau_C}\,{}_0\mathrm{I}_t+\frac{\tau_\nu}{\tau_L\tau_\mu}\,{}_0\mathrm{I}_t^{1+\mu-\nu}+\frac{1}{\tau_\mu}\,{}_0\mathrm{I}_t^{1+\mu}\bigg)i(t)=\bigg(\frac{\tau_\nu}{\tau_L}\,{}_0\mathrm{D}_t^{\nu}+1\bigg)\mathcal{E}(t), \tag{6}$$

governing the behavior of generative-generative RLC circuit is obtained, while dissipative-generative and generative-dissipative RLC circuits are described by

$$R\bigg(\tau_C\tau_\nu\,{}_0\mathrm{D}_t^{2+\nu}+\tau_\alpha\tau_\nu\,{}_0\mathrm{D}_t^{1+\alpha+\nu}+\frac{\tau_C\tau_\nu}{\tau_L}\,{}_0\mathrm{D}_t^{1+\nu}+\tau_C\,\frac{\mathrm{d}}{\mathrm{d}t}+\frac{\tau_\alpha\tau_\nu}{\tau_L}\,{}_0\mathrm{D}_t^{\alpha+\nu}+\tau_\alpha\,{}_0\mathrm{D}_t^{\alpha}+\frac{\tau_\nu}{\tau_L}\,{}_0\mathrm{D}_t^{\nu}+1\bigg)i(t)$$
$$=\bigg(\frac{\tau_C\tau_\nu}{\tau_L}\,{}_0\mathrm{D}_t^{1+\nu}+\tau_C\,\frac{\mathrm{d}}{\mathrm{d}t}+\frac{\tau_\alpha\tau_\nu}{\tau_L}\,{}_0\mathrm{D}_t^{\alpha+\nu}+\tau_\alpha\,{}_0\mathrm{D}_t^{\alpha}\bigg)\mathcal{E}(t), \tag{7}$$

and

$$R\left(\tau_L\,\frac{\mathrm{d}}{\mathrm{d}t}+\tau_\beta\,{}_0\mathrm{D}_t^{\beta}+1+\frac{1}{\tau_C}\,{}_0\mathrm{I}_t+\frac{1}{\tau_\mu}\,{}_0\mathrm{I}_t^{1+\mu}\right)i(t)=\mathcal{E}(t), \tag{8}$$

respectively, former by employing constitutive equations of dissipative capacitor and generative inductor (1) and (4), and latter by the use of generative capacitor and dissipative inductor models (2) and (3). Governing equations (5) - (8) share the same notation: ${}_0\mathrm{D}_t^{n+\xi}$, with $n\in\mathbb{N}_0$ and $\xi\in(0,1)$, denotes the operator of Riemann-Liouville fractional differentiation, defined as in [23] by

$${}_0\mathrm{D}_t^{n+\xi}f\,(t)=\frac{\mathrm{d}^{n+1}}{\mathrm{d}t^{n+1}}\,{}_0\mathrm{I}_t^{1-\xi}f\,(t)=\frac{\mathrm{d}^{n+1}}{\mathrm{d}t^{n+1}}\left(\frac{t^{-\xi}}{\Gamma\,(1-\xi)}*f\,(t)\right),$$

$\mathcal{E}$ is the electromotive force, R denotes resistor's resistance, $\tau_C=RC\,[\mathrm{s}]$ and $\tau_L=\frac{L}{R}\,[\mathrm{s}]$ are classical time constants, while $\tau_\alpha=RC_\alpha\,[\mathrm{s}^\alpha]$, $\tau_\mu=RC_\mu\,[\mathrm{s}^{1+\mu}]$, $\tau_\beta=\frac{L_\beta}{R}\,[\mathrm{s}^\beta]$, and $\tau_\nu=\frac{L_\nu}{R}\,[\mathrm{s}^{1+\nu}]$ are fractional time constants.

Modeling electrical devices utilized for storing energy, like supercapacitors, ultracapacitors, and electrochemical double-layer capacitors (EDLC), require the use of nonclassical constitutive models and the application of fractional calculus proved to be useful in formulating constitutive equations for such devices. In particular, the soundness of fractional order models of electric elements is discussed in [51] regarding their physical properties. The review of supercapacitor's models involving fractional calculus along with their application is presented in [2], while [43] reviews the characteristics of electric elements of

fractional order, as well as the possibilities of their modeling, realizations, and applications. Mathematically, the behavior of supercapacitors and ultracapacitors is described either by linear constitutive models, see [8, 33, 34], or by the nonlinear constitutive equations, see [10]. Moreover, the constitutive equation of fractional capacitor may also involve fractional differentiation orders higher than one, as in [20]. The experimental work includes testing of supercapacitors at various frequencies and comparison of obtained results with the theoretical models, see [1, 22], or even manufacturing electric elements of fractional order, see [21, 24, 28], as well as their realizations by the use of constant phase element, as demonstrated in [5, 6]. The modeling of electrochemical double-layer capacitors also includes the fractional calculus, that is investigated in [19] through the frequency characteristics, in [26, 35] through the time domain analysis, and in [27] by the analysis of capacitor's quality properties. The experiments conducted in [3] aimed to test the presence of hereditariness effects in electric double-layer capacitors. Fractional order models of the memory effects in inductor are discussed in [25, 42, 48], while [41, 53] investigate the complex electric networks containing electric elements of fractional order. Derivation of elements' constitutive models from Maxwell's equations and models of material can be found in [29, 46, 47].

The equations describing time domain behavior of RLC and RC circuits are generalized in [12, 13] by the simple replacement of the integer order derivatives by the fractional ones, while the transient response investigations of the series RC_α circuit, as well of the series and parallel $RL_\beta C_\alpha$ are conducted in [16, 17, 18], where the fractional models of capacitor and inductor are taken into account. The analytical tools in obtaining the time domain response of electrical circuits containing fractional capacitor and inductor are applied in [4], while [7, 44, 45] use numerical tools for the same purpose. The analysis of $RL_\beta C_\alpha$ and fractional RC, RL, and LC circuits in the frequency domain is performed in [37, 38, 39], while [9, 40] investigate the Wien bridge oscillators. Fractional order filters, like the Kalman filter, and filter realizations are studied in [30, 49], while [36, 50] deal with the resonance phenomena in fractional electric circuits.

Comprehensive material regarding the modeling of classical and fractional systems, signal propagation, and fractional order circuits is contained in [31, 32, 52].

2 Model formulation

In order to derive governing equations (5) - (8), the second Kirchhoff's law, combined with Ohm's law,

$$\mathcal{E}(t) = R\, i(t) + u_L(t) + u_C(t) \tag{9}$$

is coupled with constitutive models of dissipative/generative capacitor and inductor, that rewritten in terms of current and voltage for dissipative elements modeled by (1) and (3) are obtained as

$$i(t) = C\,\frac{\mathrm{d}}{\mathrm{d}t}u_C(t) + C_\alpha\, {}_0\mathrm{D}_t^\alpha u_C(t), \tag{10}$$

$$u_L(t) = L\,\frac{\mathrm{d}}{\mathrm{d}t}i(t) + L_\beta\, {}_0\mathrm{D}_t^\beta i(t), \tag{11}$$

by differentiation and use of defining relation of current $i(t) = \frac{\mathrm{d}}{\mathrm{d}t}q(t)$ and Faraday's law of electromagnetic induction $u_L(t) = \frac{\mathrm{d}}{\mathrm{d}t}\phi(t)$, while constitutive equations (2) and (4) of generative elements are rewritten as

$$u_C(t) = \frac{1}{C}\,\mathrm{I}_t i(t) + \frac{1}{C_\mu}\,\mathrm{I}_t^{1+\mu} i(t), \tag{12}$$

$$i(t) = \frac{1}{L}\,\mathrm{I}_t u_L(t) + \frac{1}{L_\nu}\,\mathrm{I}_t^{1+\nu} u_L(t), \tag{13}$$

by the use of $q(t) = \int_0^t i(t')\mathrm{d}t' = {}_0\mathrm{I}_t^1 i(t)$ and $\phi(t) = \int_0^t u_L(t')\mathrm{d}t' = {}_0\mathrm{I}_t^1 u_L(t)$, provided that $q(0) = 0$ and $\phi(0) = 0$, along with the semi-group property for fractional integrals, i.e., ${}_0\mathrm{I}_t^\xi\, {}_0\mathrm{I}_t^\zeta = {}_0\mathrm{I}_t^\zeta\, {}_0\mathrm{I}_t^\xi = {}_0\mathrm{I}_t^{\xi+\zeta}$.

Governing equation of the dissipative-dissipative RLC circuit in the complex domain takes the form

$$R\left(\tau_L\tau_C s^2 + \tau_L\tau_\alpha s^{1+\alpha} + \tau_C\tau_\beta s^{1+\beta} + \tau_\alpha\tau_\beta s^{\alpha+\beta} + \tau_C s + \tau_\alpha s^\alpha + 1\right)\hat{i}(s) = \left(\tau_C s + \tau_\alpha s^\alpha\right)\hat{\mathcal{E}}(s),$$

implying the transfer function

$$\hat{g}_i^{(\mathrm{dd})}(s) = \frac{\hat{i}(s)}{\hat{\mathcal{E}}(s)} = \frac{1}{R}\,\frac{\tau_C s + \tau_\alpha s^\alpha}{\Phi_{\mathrm{dd}}(s)}, \quad \text{with} \tag{14}$$

$$\Phi_{\mathrm{dd}}(s) = \tau_L\tau_C s^2 + \tau_L\tau_\alpha s^{1+\alpha} + \tau_C\tau_\beta s^{1+\beta} + \tau_\alpha\tau_\beta s^{\alpha+\beta} + \tau_C s + \tau_\alpha s^\alpha + 1,$$

and it is obtained by coupling the Laplace transforms of the second Kirchhoff's law (9) and constitutive models of dissipative capacitor (10) and inductor (11), yielding

$$\hat{\mathcal{E}}(s) = R\,\hat{i}(s) + \hat{u}_L(s) + \hat{u}_C(s) \tag{15}$$

and

$$\hat{i}(s) = (C\,s + C_\alpha\,s^\alpha)\,\hat{u}_C(s), \tag{16}$$

$$\hat{u}_L(s) = \left(L\,s + L_\beta\,s^\beta\right)\hat{i}(s), \tag{17}$$

respectively, where the Laplace transform, defined as

$$\hat{f}(s) = \mathcal{L}[f(t)](s) = \int_0^\infty f(t)\,\mathrm{e}^{-st}\mathrm{d}t, \quad \text{for} \quad \mathrm{Re}s > 0,$$

is used along with the Laplace transforms of Riemann-Liouville fractional derivative and fractional integral

$$\mathcal{L}\left[{}_0\mathrm{D}_t^\xi f\,(t)\right](s) = s^\xi\hat{f}(s) - \left[{}_0\mathrm{I}_t^{1-\xi} f\,(t)\right]_{t=0} = s^\xi\hat{f}(s) \quad \text{and} \quad \mathcal{L}\left[{}_0\mathrm{I}_t^\xi f\,(t)\right](s) = \frac{1}{s^\xi}\hat{f}(s),$$

holding for f bounded at zero, and by taking into account defining relations for classical and fractional time constants as well. Analogously, by taking the Laplace transform of constitutive equations (12) for generative capacitor and (13) for generative inductor, one has

$$\hat{u}_C(s) = \left(\frac{1}{C\,s} + \frac{1}{C_\mu\,s^{1+\mu}}\right)\hat{i}(s), \tag{18}$$

$$\hat{i}(s) = \left(\frac{1}{L\,s} + \frac{1}{L_\nu\,s^{1+\nu}}\right)\hat{u}_L(s), \tag{19}$$

that coupled with the second Kirchhoff's law in complex domain (15) and by the use of defining relations for time constants yields the governing equation of generative-generative RLC circuit in the form

$$R\Bigg(\tau_\nu s^{1+\nu} + \frac{\tau_\nu}{\tau_L}s^\nu + 1 + \frac{\tau_\nu}{\tau_L\tau_C}\frac{1}{s^{1-\nu}} + \frac{1}{\tau_C}\frac{1}{s} + \frac{\tau_\nu}{\tau_L\tau_\mu}\frac{1}{s^{1+\mu-\nu}} + \frac{1}{\tau_\mu}\frac{1}{s^{1+\mu}}\Bigg)\hat{i}(s) = \left(\frac{\tau_\nu}{\tau_L}s^\nu + 1\right)\hat{\mathcal{E}}(s),$$

so as the transfer function

$$\hat{g}_i^{(\mathrm{gg})}(s) = \frac{\hat{i}(s)}{\hat{\mathcal{E}}(s)} = \frac{1}{R}\tau_C\tau_\mu s^{1+\mu}\frac{\tau_\nu s^\nu + \tau_L}{\Phi_{\mathrm{gg}}(s)}, \quad \text{with} \tag{20}$$

$$\Phi_{\mathrm{gg}}(s) = \tau_L\tau_C\tau_\mu\tau_\nu s^{2+\mu+\nu} + \tau_C\tau_\mu\tau_\nu s^{1+\mu+\nu} + \tau_L\tau_C\tau_\mu s^{1+\mu} + \tau_\mu\tau_\nu s^{\mu+\nu} + \tau_L\tau_\mu s^\mu + \tau_C\tau_\nu s^\nu + \tau_L\tau_C.$$

Equations in complex domain governing the dissipative-generative and generative-dissipative RLC circuits

$$R\Bigg(\tau_C\tau_\nu s^{2+\nu} + \tau_\alpha\tau_\nu s^{1+\alpha+\nu} + \frac{\tau_C\tau_\nu}{\tau_L}s^{1+\nu} + \tau_C s + \frac{\tau_\alpha\tau_\nu}{\tau_L}s^{\alpha+\nu} + \tau_\alpha s^\alpha + \frac{\tau_\nu}{\tau_L}s^\nu + 1\Bigg)\hat{i}(s) = \left(\frac{\tau_C\tau_\nu}{\tau_L}s^{1+\nu} + \tau_C s + \frac{\tau_\alpha\tau_\nu}{\tau_L}s^{\alpha+\nu} + \tau_\alpha s^\alpha\right)\hat{\mathcal{E}}(s), \tag{21}$$

and

$$R\left(\tau_L s + \tau_\beta s^\beta + 1 + \frac{1}{\tau_C}\frac{1}{s} + \frac{1}{\tau_\mu}\frac{1}{s^{1+\mu}}\right)\hat{i}(s) = \hat{\mathcal{E}}(s), \tag{22}$$

along with the transfer functions

$$\hat{g}_i^{(\mathrm{dg})}(s) = \frac{\hat{i}(s)}{\hat{\mathcal{E}}(s)} = \frac{1}{R}\frac{\tau_C\tau_\nu s^{1+\nu} + \tau_L\tau_C s + \tau_\alpha\tau_\nu s^{\alpha+\nu} + \tau_L\tau_\alpha s^\alpha}{\Phi_{\mathrm{dg}}(s)}, \quad \text{with} \tag{23}$$

$$\Phi_{\mathrm{dg}}(s) = \tau_L\tau_C\tau_\nu s^{2+\nu} + \tau_L\tau_\alpha\tau_\nu s^{1+\alpha+\nu} + \tau_C\tau_\nu s^{1+\nu} + \tau_L\tau_C s + \tau_\alpha\tau_\nu s^{\alpha+\nu} + \tau_L\tau_\alpha s^\alpha + \tau_\nu s^\nu + \tau_L$$

and

$$\hat{g}_i^{(\mathrm{gd})}(s) = \frac{\hat{i}(s)}{\hat{\mathcal{E}}(s)} = \frac{1}{R}\frac{\tau_C\tau_\mu s^{1+\mu}}{\Phi_{\mathrm{gd}}(s)}, \quad \text{with} \tag{24}$$
$$\Phi_{\mathrm{gd}}(s) = \tau_L\tau_C\tau_\mu s^{2+\mu} + \tau_C\tau_\beta\tau_\mu s^{1+\beta+\mu} + \tau_C\tau_\mu s^{1+\mu} + \tau_\mu s^\mu + \tau_C,$$

corresponding to governing equations (21) and (22) respectively, are obtained as a consequence of the second Kirchhoff's law (15) combined either with the constitutive equations of dissipative capacitor (16) and generative inductor (19), or with the models of generative capacitor (18) and dissipative inductor (17), where the definitions of classical and fractional time constants are used as well.

3 Thermodynamical considerations in the steady state regime

In order to analyze energy consumption/production properties of fractional RLC circuits containing dissipative and/or generative elements, the steady state regime of circuits is assumed, i.e., the electromotive force, circuits' current, and voltages of dissipative/generative capacitor and inductor are assumed as harmonic functions of angular frequency ω as

$$\underline{\mathcal{E}}(t) = \mathcal{E}_0\,\mathrm{e}^{\mathrm{j}\omega t}, \quad \underline{\mathrm{i}}(t) = i_0\,\mathrm{e}^{\mathrm{j}(\omega t+\phi_i)}, \quad \underline{\mathrm{u}}_C(t) = u_{C0}\,\mathrm{e}^{\mathrm{j}(\omega t+\phi_C)}, \quad \text{and} \quad \underline{\mathrm{u}}_L(t) = u_{L0}\,\mathrm{e}^{\mathrm{j}(\omega t+\phi_L)}, \tag{25}$$

where $\mathcal{E}_0$, i_0, u_{C0}, and u_{L0} are amplitudes and ϕ_i, ϕ_C, and ϕ_L are phase angles. Electromotive force and current, assumed as $(25)_1$ and $(25)_2$, when plugged into governing equations (5) - (8) of fractional RLC circuits, lead to the sine and cosine of current's phase angle ϕ_i, expressed in terms of ratio of current and electromotive force amplitudes $\frac{i_0}{\mathcal{E}_0}$, due to the linearity of governing equations, properties of integer order derivatives, and large time asymptotics of Riemann-Liouville fractional derivative and fractional integral, being given by

$${}_0\mathrm{D}_t^\xi\,\mathrm{e}^{\mathrm{j}(\omega t+\phi)} = (\mathrm{j}\omega)^\xi\,\mathrm{e}^{\mathrm{j}(\omega t+\phi)} = \omega^\xi\,\mathrm{e}^{\mathrm{j}(\omega t+\phi+\frac{\xi\pi}{2})} \ \text{ as } \ t\to\infty, \tag{26}$$
$${}_0\mathrm{I}_t^\xi\,\mathrm{e}^{\mathrm{j}(\omega t+\phi)} = \frac{1}{(\mathrm{j}\omega)^\xi}\,\mathrm{e}^{\mathrm{j}(\omega t+\phi)} = \frac{1}{\omega^\xi}\,\mathrm{e}^{\mathrm{j}(\omega t+\phi-\frac{\xi\pi}{2})} \ \text{ as } \ t\to\infty, \tag{27}$$

see [11]. The same result would be achieved by substituting $s = \mathrm{j}\omega$ into the transfer functions (14), (20), (23), and (24), followed by the separation of real and imaginary parts in such obtained expressions, assuming $\hat{i}(\mathrm{j}\omega) = i_0\,\mathrm{e}^{\mathrm{j}(\omega t+\phi_i)}$ and $\hat{\mathcal{E}}(\mathrm{j}\omega) = \mathcal{E}_0\,\mathrm{e}^{\mathrm{j}(\omega t+\phi_i)}$.

The sign of current's phase angle cosine determines whether circuit dissipates or generates energy, since the energy consumed/produced by the fractional RLC circuit during one period T of harmonic functions (25) is determined by

$$W = \int_{nT}^{(n+1)T} \mathcal{E}(t)\,i(t)\,\mathrm{d}t = \mathcal{E}_0 i_0 \int_{nT}^{(n+1)T} \cos(\omega t)\cos(\omega t+\phi_i)\,\mathrm{d}t = \frac{1}{2}\mathcal{E}_0 i_0 T\cos\phi_i, \tag{28}$$

where

$$\mathcal{E} = \mathrm{Re}\,\underline{\mathcal{E}} \quad \text{and} \quad i = \mathrm{Re}\,\underline{\mathrm{i}},$$

while the sign of phase angle sine determines whether the circuit has capacitive or inductive character, so that if $\cos\phi_i > 0$ ($\cos\phi_i < 0$), then circuit dissipates (generates) energy and if $\sin\phi_i > 0$ ($\sin\phi_i < 0$), then circuit has capacitive (inductive) character, since current leads (lags) the electromotive force.

Rather than plugging harmonic electromotive force and current into governing equations, harmonic current and appropriate harmonic voltage are inserted into constitutive equations for dissipative elements (10) and (11) yielding dissipative capacitor's admittance and dissipative inductor's impedance as

$$Y_C^{(\mathrm{d})}(\omega) = \frac{\underline{\mathrm{i}}(t)}{\underline{\mathrm{u}}_C(t)} = C\,\omega\,\mathrm{e}^{\mathrm{j}\frac{\pi}{2}} + C_\alpha\,\omega^\alpha\,\mathrm{e}^{\mathrm{j}\frac{\alpha\pi}{2}},$$
$$Z_L^{(\mathrm{d})}(\omega) = \frac{\underline{\mathrm{u}}_L(t)}{\underline{\mathrm{i}}(t)} = L\,\omega\,\mathrm{e}^{\mathrm{j}\frac{\pi}{2}} + L_\beta\,\omega^\beta\,\mathrm{e}^{\mathrm{j}\frac{\beta\pi}{2}},$$

by the large time asymptotics of Riemann-Liouville fractional derivative (26), so that

$$\frac{1}{Y_C^{(\mathrm{d})}(\omega)} = \frac{C_\alpha\omega^\alpha\cos\frac{\alpha\pi}{2} - \mathrm{j}\left(C\omega + C_\alpha\omega^\alpha\sin\frac{\alpha\pi}{2}\right)}{C^2\omega^2 + 2CC_\alpha\omega^{1+\alpha}\sin\frac{\alpha\pi}{2} + C_\alpha^2\omega^{2\alpha}}, \tag{29}$$

$$Z_L^{(\mathrm{d})}(\omega) = L_\beta \omega^\beta \cos\frac{\beta\pi}{2} + \mathrm{j}\left(L\omega + L_\beta\omega^\beta \sin\frac{\beta\pi}{2}\right), \tag{30}$$

while generative capacitor's impedance and generative inductor's admittance

$$Z_C^{(\mathrm{g})}(\omega) = \frac{\underline{\mathrm{u}}_C(t)}{\underline{\mathrm{i}}(t)} = \frac{1}{C}\frac{1}{\omega \mathrm{e}^{\mathrm{j}\frac{\pi}{2}}} + \frac{1}{C_\mu}\frac{1}{\omega^{1+\mu}\mathrm{e}^{\mathrm{j}\frac{(1+\mu)\pi}{2}}},$$
$$Y_L^{(\mathrm{g})}(\omega) = \frac{\underline{\mathrm{i}}(t)}{\underline{\mathrm{u}}_L(t)} = \frac{1}{L}\frac{1}{\omega \mathrm{e}^{\mathrm{j}\frac{\pi}{2}}} + \frac{1}{L_\nu}\frac{1}{\omega^{1+\nu}\mathrm{e}^{\mathrm{j}\frac{(1+\nu)\pi}{2}}},$$

are obtained using large time asymptotics of the fractional integral (27) in generative capacitor's and inductor's models (12) and (13), so that

$$Z_C^{(\mathrm{g})}(\omega) = -\frac{\sin\frac{\mu\pi}{2}}{C_\mu\omega^{1+\mu}} - \mathrm{j}\left(\frac{1}{C\omega} + \frac{\cos\frac{\mu\pi}{2}}{C_\mu\omega^{1+\mu}}\right), \tag{31}$$

$$\frac{1}{Y_L^{(\mathrm{g})}(\omega)} = -LL_\nu\omega^{1+\nu}\frac{L\sin\frac{\nu\pi}{2} - \mathrm{j}\left(L_\nu\omega^\nu + L\cos\frac{\nu\pi}{2}\right)}{L_\nu^2\omega^{2\nu} + 2LL_\nu\omega^\nu\cos\frac{\nu\pi}{2} + L^2}. \tag{32}$$

The second Kirchhoff's law (9) in the steady state regime

$$\underline{\mathcal{E}}(t) = R\,\underline{\mathrm{i}}(t) + \underline{\mathrm{u}}_L(t) + \underline{\mathrm{u}}_C(t), \quad \text{i.e.,} \quad \underline{\mathcal{E}}(t) = Z_e\,\underline{\mathrm{i}}(t), \tag{33}$$

with $Z_e = R + Z_C + Z_L$ being the equivalent impedance of the fractional RLC circuit, using $(25)_{1,2}$ yields

$$Z_e = \frac{\mathcal{E}_0}{i_0}\,\mathrm{e}^{-\mathrm{j}\phi_i} \quad \text{implying} \quad \cos\phi_i = \frac{\mathrm{Re}\,Z_e}{|Z_e|} \quad \text{and} \quad \sin\phi_i = -\frac{\mathrm{Im}\,Z_e}{|Z_e|}, \tag{34}$$

so that in the case of dissipative-dissipative RLC circuit the equivalent impedance

$$Z_e^{(\mathrm{dd})}(\omega) = R + \frac{1}{Y_C^{(\mathrm{d})}(\omega)} + Z_L^{(\mathrm{d})}(\omega) \tag{35}$$

gives

$$\cos\phi_i^{(\mathrm{dd})}(\omega) = \frac{1}{|Z_e^{(\mathrm{dd})}(\omega)|}\left(R + \frac{C_\alpha\omega^\alpha\cos\frac{\alpha\pi}{2}}{C^2\omega^2 + 2CC_\alpha\omega^{1+\alpha}\sin\frac{\alpha\pi}{2} + C_\alpha^2\omega^{2\alpha}} + L_\beta\omega^\beta\cos\frac{\beta\pi}{2}\right), \tag{36}$$

$$\sin\phi_i^{(\mathrm{dd})}(\omega) = \frac{1}{|Z_e^{(\mathrm{dd})}(\omega)|}\left(\frac{C\omega + C_\alpha\omega^\alpha\sin\frac{\alpha\pi}{2}}{C^2\omega^2 + 2CC_\alpha\omega^{1+\alpha}\sin\frac{\alpha\pi}{2} + C_\alpha^2\omega^{2\alpha}} - L\omega - L_\beta\omega^\beta\sin\frac{\beta\pi}{2}\right), \tag{37}$$

using (34) along with capacitor's and inductor's impedances (29) and (30). Clearly, the circuit is dissipative for all frequencies since $\cos\phi_i > 0$, see (36), having the asymptotics

$$\cos\phi_i^{(\mathrm{dd})}(\omega) \sim \cos\frac{\alpha\pi}{2} \quad \text{as} \quad \omega\to 0 \quad \text{and} \quad \cos\phi_i^{(\mathrm{dd})}(\omega) \sim \frac{L_\beta}{L}\frac{1}{\omega^{1-\beta}}\cos\frac{\beta\pi}{2} \to 0^+ \quad \text{as} \quad \omega\to\infty, \tag{38}$$

while its character changes from capacitive for low frequencies to inductive for high frequencies, due to the low and high frequency asymptotics of phase angle sine

$$\sin\phi_i^{(\mathrm{dd})}(\omega) \sim \sin\frac{\alpha\pi}{2} > 0 \quad \text{as} \quad \omega\to 0 \quad \text{and} \quad \sin\phi_i^{(\mathrm{dd})}(\omega) \sim -1 \quad \text{as} \quad \omega\to\infty. \tag{39}$$

The phase angle cosine and sine as functions of the angular frequency, obtained by (36) and (37), are depicted in Figure 1, illustrating that the dissipative-dissipative RLC circuit consumes energy for all frequencies, with the possibility that the phase angle cosine may even have an additional minimum, compare Figures 1a and 1b, nevertheless slowly tending to zero from above, as predicted by the asymptotics (38), while the phase angle sine either monotonically or non-monotonically changes from positive to negative values inferring the change of circuit's character from capacitive to inductive, as predicted by the asymptotics (39).

The equivalent impedance of the generative-generative fractional RLC circuit

$$Z_e^{(\mathrm{gg})}(\omega) = R + Z_C^{(\mathrm{g})}(\omega) + \frac{1}{Y_L^{(\mathrm{g})}(\omega)}, \tag{40}$$

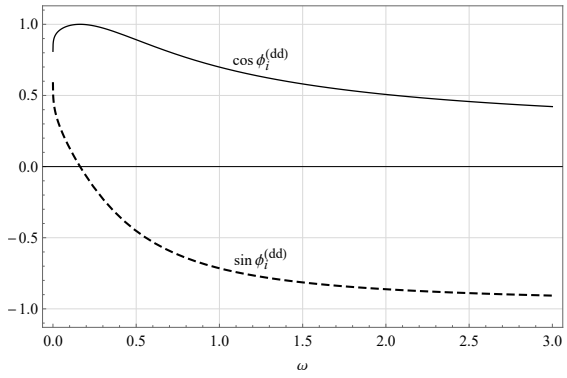

(a) Curves obtained for model parameters as below and $\tau_\alpha = 3$.

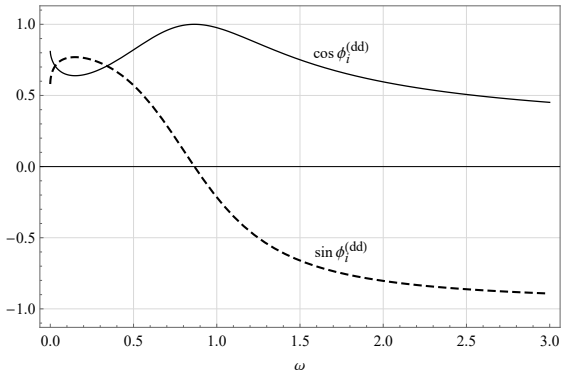

(b) Curves obtained for model parameters as below and $\tau_\alpha = 0.2$.

Figure 1: Energy consumption/production properties and capacitive/inductive character of the dissipative-dissipative RLC circuit: $\cos\phi_i^{(\mathrm{dd})}$ and $\sin\phi_i^{(\mathrm{dd})}$ as functions of angular frequency ω, obtained for model parameters: $\alpha = 0.4$, $\beta = 0.8$, $\tau_C = 0.5$, $\tau_L = 0.5$, and $\tau_\beta = 1.5$.

using (34) together with capacitor's and inductor's impedances (31) and (32) yields

$$\cos\phi_i^{(\mathrm{gg})}(\omega) = \frac{1}{|Z_e^{(\mathrm{gg})}(\omega)|}\left(R - \frac{\sin\frac{\mu\pi}{2}}{C_\mu\omega^{1+\mu}} - LL_\nu\omega^{1+\nu}\frac{L\sin\frac{\nu\pi}{2}}{L_\nu^2\omega^{2\nu} + 2LL_\nu\omega^\nu\cos\frac{\nu\pi}{2} + L^2}\right), \tag{41}$$

$$\sin\phi_i^{(\mathrm{gg})}(\omega) = \frac{1}{|Z_e^{(\mathrm{gg})}(\omega)|}\left(\frac{1}{C\omega} + \frac{\cos\frac{\mu\pi}{2}}{C_\mu\omega^{1+\mu}} - LL_\nu\omega^{1+\nu}\frac{L_\nu\omega^\nu + L\cos\frac{\nu\pi}{2}}{L_\nu^2\omega^{2\nu} + 2LL_\nu\omega^\nu\cos\frac{\nu\pi}{2} + L^2}\right), \tag{42}$$

inferring that circuit is generative for both low and high frequencies and may be dissipative for mid-range frequencies, due to

$$\cos\phi_i^{(\mathrm{gg})}(\omega) \sim -\sin\frac{\mu\pi}{2} < 0 \quad \text{as} \quad \omega\to 0 \quad \text{and} \quad \cos\phi_i^{(\mathrm{gg})}(\omega) \sim -\frac{L}{L_\nu\omega^\nu}\sin\frac{\nu\pi}{2} \to 0^- \quad \text{as} \quad \omega\to\infty, \tag{43}$$

and, as for the dissipative-dissipative RLC circuit, capacitive properties prevail for low frequencies, while the circuit is inductive for high frequencies, since

$$\sin\phi_i^{(\mathrm{gg})}(\omega) \sim \cos\frac{\mu\pi}{2} > 0 \quad \text{as} \quad \omega\to 0 \quad \text{and} \quad \sin\phi_i^{(\mathrm{gg})}(\omega) \sim -1 \quad \text{as} \quad \omega\to\infty. \tag{44}$$

Figure 2 depicts the phase angle cosine and sine versus the angular frequency for the generative-generative RLC circuit, obtained according to (41) and (42), where the energy is produced for all frequencies in the case of model parameters used to obtain the plot from Figure 2c, while in the other two cases, the energy is produced for both low and high frequencies, see Figures 2a and 2b, that is in accordance with the asymptotics (43), while the circuit consumes energy for the mid-range frequencies, with the possibility of the abrupt change in energy consumption/production properties, as illustrated in Figure 2b. The change of circuit's predominant character from capacitive to inductive, see also the asymptotics (44), is non-monotonic for all depicted cases of model parameters, again with the possibility of the abrupt character change.

The equivalent impedances corresponding to the dissipative-generative and generative-dissipative RLC circuits are

$$Z_e^{(\mathrm{dg})}(\omega) = R + \frac{1}{Y_C^{(\mathrm{d})}(\omega)} + \frac{1}{Y_L^{(\mathrm{g})}(\omega)} \quad \text{and} \quad Z_e^{(\mathrm{gd})}(\omega) = R + Z_C^{(\mathrm{g})}(\omega) + Z_L^{(\mathrm{d})}(\omega), \tag{45}$$

so that for the dissipative-generative RLC circuit the equivalent impedance $Z_e^{(\mathrm{dg})}$, given by $(45)_1$, with capacitor's and inductor's impedances (29) and (32), according to (34) gives

$$\cos\phi_i^{(\mathrm{dg})}(\omega) = \frac{1}{|Z_e^{(\mathrm{dg})}(\omega)|}$$

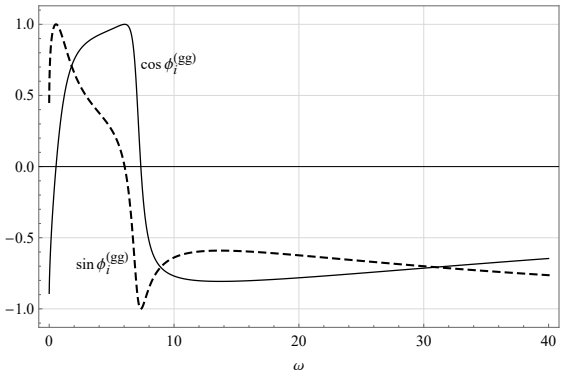

(a) Curves obtained for model parameters as below and $\tau_\mu = 2.5$.

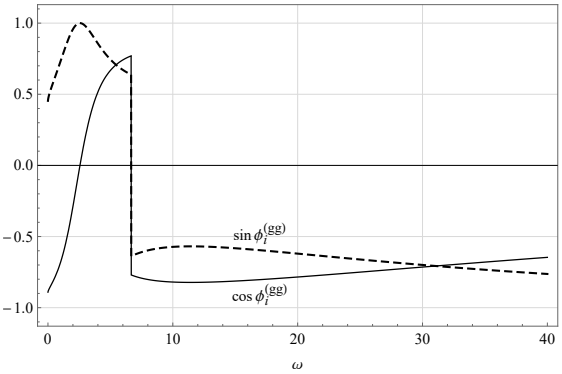

(b) Curves obtained for model parameters as below and $\tau_\mu = 0.20980\ldots$

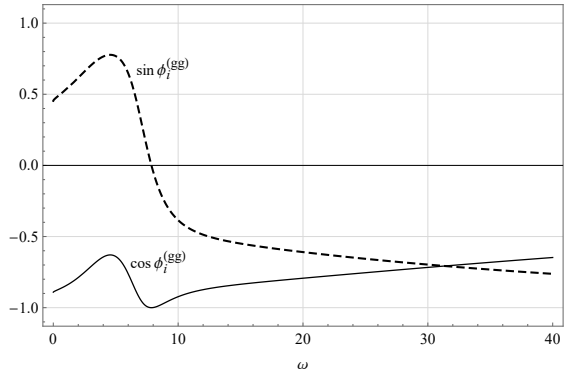

(c) Curves obtained for model parameters as below and $\tau_\mu = 0.055$.

Figure 2: Energy consumption/production properties and capacitive/inductive character of the generative-generative *RLC* circuit: $\cos\phi_i^{(\mathrm{gg})}$ and $\sin\phi_i^{(\mathrm{gg})}$ as functions of angular frequency ω, obtained for model parameters: $\mu = 0.7$, $\nu = 0.9$, $\tau_C = 0.75$, $\tau_L = 0.75$, and $\tau_\nu = 0.025$.

$$\times\left(R+\frac{C_\alpha\omega^\alpha\cos\frac{\alpha\pi}{2}}{C^2\omega^2+2CC_\alpha\omega^{1+\alpha}\sin\frac{\alpha\pi}{2}+C_\alpha^2\omega^{2\alpha}}-LL_\nu\omega^{1+\nu}\frac{L\sin\frac{\nu\pi}{2}}{L_\nu^2\omega^{2\nu}+2LL_\nu\omega^\nu\cos\frac{\nu\pi}{2}+L^2}\right), \tag{46}$$

$$\sin\phi_i^{(\mathrm{dg})}(\omega)=\frac{1}{|Z_e^{(\mathrm{dg})}(\omega)|}\times\left(\frac{C\omega+C_\alpha\omega^\alpha\sin\frac{\alpha\pi}{2}}{C^2\omega^2+2CC_\alpha\omega^{1+\alpha}\sin\frac{\alpha\pi}{2}+C_\alpha^2\omega^{2\alpha}}-LL_\nu\omega^{1+\nu}\frac{L_\nu\omega^\nu+L\cos\frac{\nu\pi}{2}}{L_\nu^2\omega^{2\nu}+2LL_\nu\omega^\nu\cos\frac{\nu\pi}{2}+L^2}\right), \tag{47}$$

along with their asymptotics

$$\cos\phi_i^{(\mathrm{dg})}(\omega)\sim\cos\frac{\alpha\pi}{2}>0\quad\text{as}\quad\omega\to0\quad\text{and}\quad\cos\phi_i^{(\mathrm{dg})}(\omega)\sim-\frac{L}{L_\nu\omega^\nu}\sin\frac{\nu\pi}{2}\to0^-\quad\text{as}\quad\omega\to\infty, \tag{48}$$

$$\sin\phi_i^{(\mathrm{dg})}(\omega)\sim\sin\frac{\alpha\pi}{2}>0\quad\text{as}\quad\omega\to0\quad\text{and}\quad\sin\phi_i^{(\mathrm{dg})}(\omega)\sim-1\quad\text{as}\quad\omega\to\infty, \tag{49}$$

while for the generative-dissipative *RLC* circuit, the equivalent impedance $Z_e^{(\mathrm{gd})}$, see $(45)_2$, employing capacitor's and inductor's impedances (30) and (31), by (34) yields

$$\cos\phi_i^{(\mathrm{gd})}(\omega)=\frac{1}{|Z_e^{(\mathrm{gd})}(\omega)|}\left(R-\frac{\sin\frac{\mu\pi}{2}}{C_\mu\omega^{1+\mu}}+L_\beta\omega^\beta\cos\frac{\beta\pi}{2}\right), \tag{50}$$

$$\sin\phi_i^{(\mathrm{gd})}(\omega)=\frac{1}{|Z_e^{(\mathrm{gd})}(\omega)|}\left(\frac{1}{C\omega}+\frac{\cos\frac{\mu\pi}{2}}{C_\mu\omega^{1+\mu}}-L\omega-L_\beta\omega^\beta\sin\frac{\beta\pi}{2}\right), \tag{51}$$

having the asymptotics

$$\cos\phi_i^{(\mathrm{gd})}(\omega) \sim -\sin\frac{\mu\pi}{2} < 0 \quad \text{as} \quad \omega \to 0 \quad \text{and} \quad \cos\phi_i^{(\mathrm{gd})}(\omega) \sim \frac{L_\beta}{L}\frac{1}{\omega^{1-\beta}}\cos\frac{\beta\pi}{2} \to 0^+ \quad \text{as} \quad \omega \to \infty, \tag{52}$$

$$\sin\phi_i^{(\mathrm{gd})}(\omega) \sim \cos\frac{\mu\pi}{2} > 0 \quad \text{as} \quad \omega \to 0 \quad \text{and} \quad \sin\phi_i^{(\mathrm{gd})}(\omega) \sim -1 \quad \text{as} \quad \omega \to \infty. \tag{53}$$

Regarding the energy consumption/production properties, one concludes that the dissipative-generative RLC circuit dissipates energy for low frequencies and generates it for high frequencies, see (48), while generative-dissipative circuit behaves exactly in the opposite way, see (52). Capacitive and inductive character of both circuits remains same as in all previous cases, compare (49) and (53) with (39) and (44).

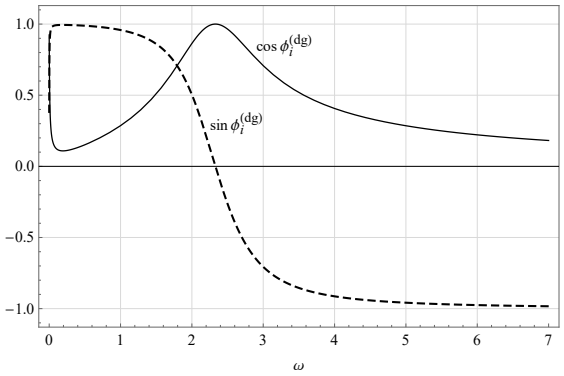

(a) Curves obtained for model parameters as below and $\tau_\nu = 5$.

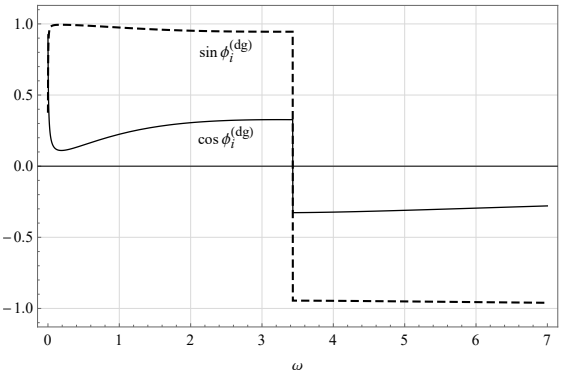

(b) Curves obtained for model parameters as below and $\tau_\nu = 0.23329\ldots$

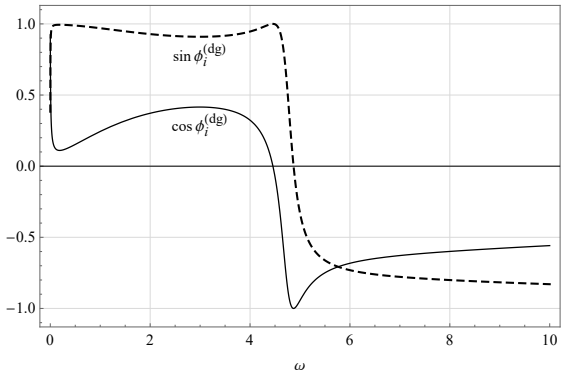

(c) Curves obtained for model parameters as below and $\tau_\nu = 0.09$.

Figure 3: Energy consumption/production properties and capacitive/inductive character of the dissipative-generative RLC circuit: $\cos\phi_i^{(\mathrm{dg})}$ and $\sin\phi_i^{(\mathrm{dg})}$ as functions of angular frequency ω, obtained for model parameters: $\alpha = 0.25$, $\nu = 0.85$, $\tau_C = 0.25$, $\tau_\alpha = 0.005$, and $\tau_L = 0.75$.

Plots of the cosine and sine of phase angle as functions of the angular frequency, shown in Figures 3 and 4, are obtained according to (46) and (47) for dissipative-generative and according to (50) and (51) for generative-dissipative RLC circuits, respectively. Figures 3a and 4c illustrate that the energy is consumed, respectively produced, for quite a large frequency range, changing the energy consumption/production properties for high frequencies in accordance with the high frequency asypmtotics (48) and (52), respectively. One notices from Figure 3a that the circuit changed its character from capacitive (capacitor is the dissipative element) to inductive (inductor is the generative element) and still being energy consuming, contrary to the case depicted in Figure 3c, where the circuit started to produce energy while still being of predominantly capacitive (dissipative) character. Figures 4a and 4c illustrate the similar behavior of the generative-dissipative RLC circuit as well, since the circuit became energy consuming while still being of predominantly capacitive character (capacitor is the generative element), see Figure 4a, contrary to the case depicted in Figure 4c, where the circuit changed its character to predominantly

inductive (inductor is the dissipative element), while still producing energy. The possibility that both types of RLC circuits suddenly change their energy consumption/production properties and predominant character is illustrated in Figures 3b and 4b.

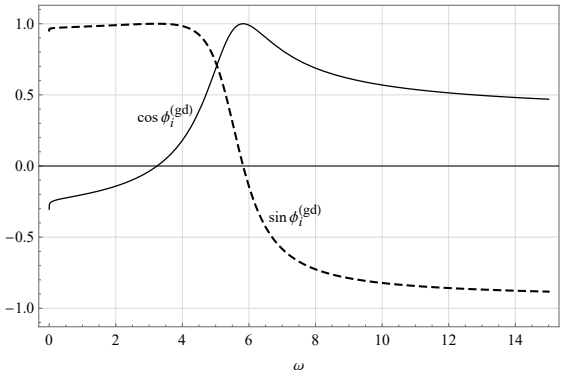

(a) Curves obtained for model parameters as below and $\tau_\beta = 5.5$.

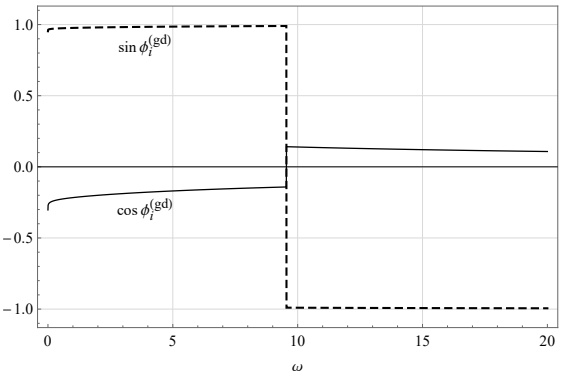

(b) Curves obtained for model parameters as below and $\tau_\beta = 0.46607\ldots$

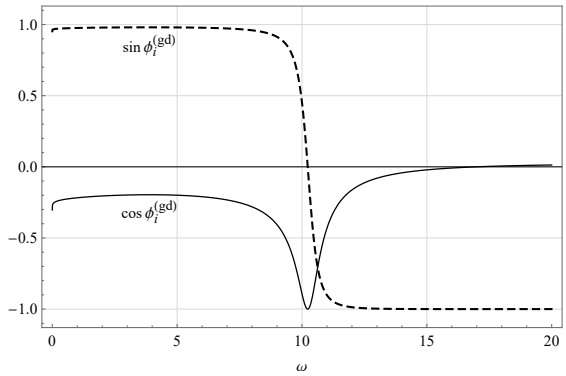

(c) Curves obtained for model parameters as below and $\tau_\beta = 0.01$.

Figure 4: Energy consumption/production properties and capacitive/inductive character of the generative-dissipative RLC circuit: $\cos\phi_i^{(\mathrm{gd})}$ and $\sin\phi_i^{(\mathrm{gd})}$ as functions of angular frequency ω, obtained for model parameters: $\mu = 0.2$, $\beta = 0.6$, $\tau_C = 0.025$, $\tau_\mu = 0.01$, and $\tau_L = 0.95$.

4 Frequency characteristics and their asymptotics

Traditionally, frequency characteristics of the transfer function modulus and argument are obtained by substituting $s = \mathrm{j}\omega$ into the transfer function and subsequently by determining its modulus and argument, where, in this particular case, the transfer function $\hat{g}_i$ takes the forms respectively given by (14), (20), (23), and (24) for the dissipative-dissipative, generative-generative, dissipative-generative, and generative-dissipative fractional RLC circuits, respectively.

However, the approach of considering the second Kirchhoff's law (33), corresponding to the fractional RLC circuit in the steady state regime, is adopted, so that the transfer function is equivalently defined by

$$\hat{g} = R\,\frac{\underline{\mathrm{i}}(t)}{\underline{\mathcal{E}}(t)} \quad \text{yielding} \quad \hat{g} = \frac{R}{Z_e} = \frac{R}{|Z_e|^2}(\mathrm{Re}\,Z_e - \mathrm{j}\,\mathrm{Im}\,Z_e) \tag{54}$$

and implying that the transfer function $\hat{g}$ is physically the equivalent admittance of the RLC circuit multiplied by resistor's resistance R. Hence, the transfer function modulus and argument, along with their asymptotics, are determined using (54) as

$$|\hat{g}\,(\omega)|_{\mathrm{dB}} = 20\log|\hat{g}(\omega)| = -10\log\left(\mathrm{Re}^2\,\frac{Z_e(\omega)}{R} + \mathrm{Im}^2\,\frac{Z_e(\omega)}{R}\right) \text{ and } \arg\hat{g}\,(\omega) = \mathrm{arccot}\,\frac{\mathrm{Re}\,Z_e(\omega)}{-\mathrm{Im}\,Z_e(\omega)}, \tag{55}$$

with the equivalent impedance Z_e given by (35) in the case of dissipative-dissipative fractional RLC circuit, expression (40) for generative-generative circuit, and by (45) for dissipative-generative and generative-dissipative circuits. Note that the definition of transfer function (54), using $\underline{\mathrm{i}}$ and $\underline{\mathcal{E}}$ given by (25), also implies

$$\hat{g} = R\,\frac{i_0}{\mathcal{E}_0}\,\mathrm{e}^{\mathrm{j}\phi_i} \quad \text{yielding} \quad |\hat{g}|_{\mathrm{dB}} = 20\log|\hat{g}| = 20\log\frac{R\,i_0}{\mathcal{E}_0} \quad \text{and} \quad \arg\hat{g} = \phi_i.$$

4.1 Dissipative-dissipative fractional RLC circuit

Considering the dissipative-dissipative fractional RLC circuit and by rewriting the real and imaginary parts of circuit's equivalent impedance (35) in terms of the classical and fractional time constants, one has

$$\mathrm{Re}\,Z_e^{(\mathrm{dd})}(\omega) = R\left(1 + \frac{\tau_\alpha\omega^\alpha\cos\frac{\alpha\pi}{2}}{\tau_C^2\omega^2 + 2\tau_C\tau_\alpha\omega^{1+\alpha}\sin\frac{\alpha\pi}{2} + \tau_\alpha^2\omega^{2\alpha}} + \tau_\beta\omega^\beta\cos\frac{\beta\pi}{2}\right), \tag{56}$$

$$\mathrm{Im}\,Z_e^{(\mathrm{dd})}(\omega) = -R\left(\frac{\tau_C\omega + \tau_\alpha\omega^\alpha\sin\frac{\alpha\pi}{2}}{\tau_C^2\omega^2 + 2\tau_C\tau_\alpha\omega^{1+\alpha}\sin\frac{\alpha\pi}{2} + \tau_\alpha^2\omega^{2\alpha}} - \tau_L\omega - \tau_\beta\omega^\beta\sin\frac{\beta\pi}{2}\right), \tag{57}$$

yielding the transfer function modulus and argument according to (55).

Figure 5 presents frequency characteristics of the transfer function modulus and argument, i.e., Bode diagrams, for same two sets of model parameters as in the case of plots from Figure 1. The transfer function modulus, shown in Figure 5a, is a non-monotonic function of the angular frequency, tending to the negative infinity for low frequencies, implying that it has a zero of non-integer order at the origin, as obvious from the form (14) of the transfer function $\hat{g}^{(\mathrm{dd})}$. Further, the transfer function modulus attains a maximum and tends to the negative infinity for high frequencies, suggesting that the transfer function $\hat{g}^{(\mathrm{dd})}$ has a pair of complex conjugated poles, that is exactly the case for the model parameters used to produce dashed-line plot, while the parameters used for the solid-line plot yield no poles of the transfer function. The shape of the transfer function modulus suggests that the dissipative-dissipative RLC circuit behaves as the band-pass filter with different band-widths.

The transfer function argument, so as its sine, either monotonically or non-monotonically changes from positive to negative values as the angular frequency increases, as obvious from Figure 5b, implying the change of circuit's behavior from predominantly capacitive to predominantly inductive, with argument's span between $-\frac{\pi}{2}$ and $\frac{\pi}{2}$ implying dissipativity of the circuit for the whole range of frequencies, since argument's cosine is positive.

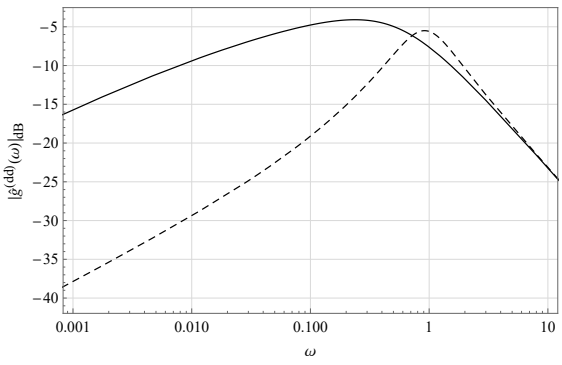

(a) Modulus of the transfer function $\hat{g}^{(\mathrm{dd})}$.

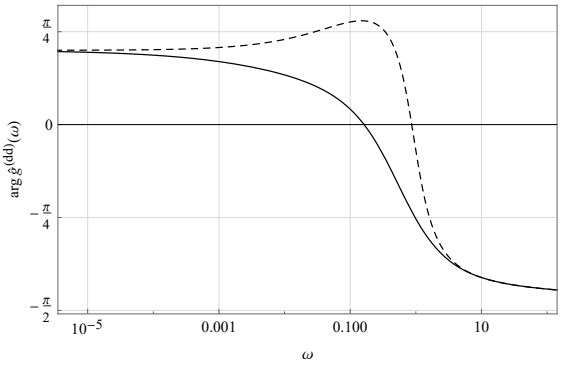

(b) Argument of the transfer function $\hat{g}^{(\mathrm{dd})}$.

Figure 5: Frequency characteristics of transfer function modulus and argument for dissipative-dissipative RLC circuit, obtained for model parameters: $\alpha = 0.4$, $\beta = 0.8$, $\tau_C = 0.5$, $\tau_L = 0.5$, $\tau_\beta = 1.5$, and $\tau_\alpha = 3$ - solid line and $\tau_\alpha = 0.2$ - dashed line.

As already noted in Section 3, the capacitive character of the fractional RLC circuit prevails for low frequencies and therefore the corresponding asymptotics of $\mathrm{Re}\,Z_e^{(\mathrm{dd})}$ and $\mathrm{Im}\,Z_e^{(\mathrm{dd})}$, given by (56) and (57), is

$$\mathrm{Re}\,Z_e^{(\mathrm{dd})}(\omega) = R\,\frac{\cos\frac{\alpha\pi}{2}}{\tau_\alpha\omega^\alpha}\begin{cases}1 + \frac{\tau_\alpha\omega^\alpha}{\cos\frac{\alpha\pi}{2}} + O(\omega^{1-\alpha}), & \text{if } \alpha \in \left(0, \frac{1}{2}\right),\\ 1 + O(\omega^{1-\alpha}), & \text{if } \alpha \in \left[\frac{1}{2}, 1\right),\end{cases} \quad \text{as} \quad \omega \to 0, \tag{58}$$

$$\operatorname{Im} Z_e^{(\mathrm{dd})}(\omega) = -R\,\frac{\sin\frac{\alpha\pi}{2}}{\tau_\alpha\omega^\alpha}\left(1+O(\omega^{1-\alpha})\right), \quad \text{as} \quad \omega\to 0, \tag{59}$$

where only the leading terms of real and imaginary parts of dissipative capacitor's impedance $\frac{1}{Y_C^{(\mathrm{d})}}$, given by (29), are taken into account, since they are of the order $-\alpha$, which is certainly smaller than the order $\beta>0$ of the leading terms of dissipative inductor's impedance $\operatorname{Re} Z_L^{(\mathrm{d})}$ and $\operatorname{Im} Z_L^{(\mathrm{d})}$, see (30), so that, by $(55)_1$, (58), and (59), for the transfer function modulus one has

$$\left|\hat g^{(\mathrm{dd})}(\omega)\right|_{\mathrm{dB}} = 20\log(\tau_\alpha\omega^\alpha) - 10\log\begin{cases}1+2\tau_\alpha\omega^\alpha\cos\frac{\alpha\pi}{2}+\tau_\alpha^2\omega^{2\alpha}+O(\omega^{1-\alpha}), & \text{if } \alpha\in\left(0,\frac13\right),\\ 1+2\tau_\alpha\omega^\alpha\cos\frac{\alpha\pi}{2}+O(\omega^{1-\alpha}), & \text{if } \alpha\in\left[\frac13,\frac12\right),\\ 1+O(\omega^{1-\alpha}), & \text{if } \alpha\in\left[\frac12,1\right),\end{cases} \quad \text{as } \omega\to 0, \tag{60}$$

while the transfer function argument, by $(55)_2$, (58), and (59), is

$$\cot\arg\hat g^{(\mathrm{dd})}(\omega) = \cot\frac{\alpha\pi}{2}\begin{cases}1+\frac{\tau_\alpha\omega^\alpha}{\cos\frac{\alpha\pi}{2}}+O(\omega^{1-\alpha}), & \text{if } \alpha\in\left(0,\frac12\right),\\ 1+O(\omega^{1-\alpha}), & \text{if } \alpha\in\left[\frac12,1\right),\end{cases} \quad \text{as} \quad \omega\to 0. \tag{61}$$

On the other hand, the inductive properties of the fractional RLC circuits are more prominent for the high frequencies and therefore $\operatorname{Re} Z_e^{(\mathrm{dd})}$ and $\operatorname{Im} Z_e^{(\mathrm{dd})}$, given by (56) and (57), are of the form

$$\operatorname{Re} Z_e^{(\mathrm{dd})}(\omega) = R\,\tau_\beta\omega^\beta\cos\frac{\beta\pi}{2}\left(1+\frac{\omega^{-\beta}}{\tau_\beta\cos\frac{\beta\pi}{2}}+O(\omega^{-1-\beta})\right), \quad \text{as} \quad \omega\to\infty, \tag{62}$$

$$\operatorname{Im} Z_e^{(\mathrm{dd})}(\omega) = R\,\tau_L\omega\left(1+\frac{\tau_\beta}{\tau_L}\omega^{-1+\beta}\sin\frac{\beta\pi}{2}+O(\omega^{-2})\right), \quad \text{as} \quad \omega\to\infty, \tag{63}$$

due to the leading terms of dissipative capacitor's impedance (29), that are

$$\operatorname{Re}\frac{1}{Y_C^{(\mathrm{d})}} \sim R\,\frac{\tau_\alpha}{\tau_C^2}\omega^{-2+\alpha}\cos\frac{\alpha\pi}{2} \quad \text{and} \quad \operatorname{Im}\frac{1}{Y_C^{(\mathrm{d})}} \sim -R\,\frac{1}{\tau_C}\omega^{-1}, \quad \text{as} \quad \omega\to\infty, \tag{64}$$

so that (62) and (63), by (55), yield the high frequency asymptotics of transfer function modulus and argument in the respective forms

$$\left|\hat g^{(\mathrm{dd})}(\omega)\right|_{\mathrm{dB}} = -20\log(\tau_L\omega) - 10\log\left(1+2\frac{\tau_\beta}{\tau_L}\omega^{-1+\beta}\sin\frac{\beta\pi}{2}+\frac{\tau_\beta^2}{\tau_L^2}\omega^{-2+2\beta}+2\frac{\tau_\beta}{\tau_L^2}\omega^{-2+\beta}\cos\frac{\beta\pi}{2}+O(\omega^{-2})\right), \tag{65}$$

$$\cot\arg\hat g^{(\mathrm{dd})}(\omega) = -\frac{\tau_\beta}{\tau_L}\omega^{-1+\beta}\cos\frac{\beta\pi}{2}\left(1-\frac{\tau_\beta}{\tau_L}\omega^{-1+\beta}\sin\frac{\beta\pi}{2} + \begin{cases}\frac{\omega^{-\beta}}{\tau_\beta\cos\frac{\beta\pi}{2}}-\frac{1}{\tau_L}\omega^{-1}\tan\frac{\beta\pi}{2}+O(\omega^{-1-\beta}), & \text{if } \beta\in\left(0,\frac13\right],\\ \frac{\omega^{-\beta}}{\tau_\beta\cos\frac{\beta\pi}{2}}-\frac{1}{\tau_L}\omega^{-1}\tan\frac{\beta\pi}{2}+\frac{\tau_\beta^2}{\tau_L^2}\omega^{-2+2\beta}\sin^2\frac{\beta\pi}{2}+O(\omega^{-1-\beta}), & \text{if } \beta\in\left(\frac13,\frac12\right],\\ \frac{\omega^{-\beta}}{\tau_\beta\cos\frac{\beta\pi}{2}}+\frac{\tau_\beta^2}{\tau_L^2}\omega^{-2+2\beta}\sin^2\frac{\beta\pi}{2}-\frac{1}{\tau_L}\omega^{-1}\tan\frac{\beta\pi}{2}+O(\omega^{-3+3\beta}), & \text{if } \beta\in\left(\frac12,\frac23\right),\\ \frac{\tau_\beta^2}{\tau_L^2}\omega^{-2+2\beta}\sin^2\frac{\beta\pi}{2}+\frac{\omega^{-\beta}}{\tau_\beta\cos\frac{\beta\pi}{2}}+O(\omega^{-3+3\beta}), & \text{if } \beta\in\left[\frac23,\frac34\right),\\ \frac{\tau_\beta^2}{\tau_L^2}\omega^{-2+2\beta}\sin^2\frac{\beta\pi}{2}+O(\omega^{-3+3\beta}), & \text{if } \beta\in\left[\frac34,1\right),\end{cases}\right) \tag{66}$$

as $\omega\to\infty$, since (62) and (63) used in $(55)_2$ yield

$$\cot\arg\hat g^{(\mathrm{dd})}(\omega) = -\frac{\tau_\beta}{\tau_L}\omega^{-1+\beta}\cos\frac{\beta\pi}{2}\left(1+\frac{\omega^{-\beta}}{\tau_\beta\cos\frac{\beta\pi}{2}}+O(\omega^{-1-\beta})\right) \times\left(1-\frac{\tau_\beta}{\tau_L}\omega^{-1+\beta}\sin\frac{\beta\pi}{2}+\frac{\tau_\beta^2}{\tau_L^2}\omega^{-2+2\beta}\sin^2\frac{\beta\pi}{2}+\begin{cases}O(\omega^{-2}), & \text{if } \beta\in\left(0,\frac13\right],\\ O(\omega^{-3+3\beta}), & \text{if } \beta\in\left(\frac13,1\right),\end{cases}\right)$$

as $\omega \to \infty$, according to the series expansion $\frac{1}{1+x} = 1 - x + x^2 + O(x^3)$ as $x \to 0$.

Transfer function modulus and argument versus the angular frequency for different values of fractional order of dissipative capacitor are depicted in Figure 6, along with their asymptotics. The transfer function modulus, see Figure 6a, is a linear function of $\log \omega$, for both low and high frequencies, with the slope either determined by the fractional order α for low frequencies, or with the slope equal to one for high frequencies, as predicted by the asymptotics formulae (60) and (65). The transfer function argument, depicted in Figure 6b, agrees very well with the low and high frequency asymptotics (61) and (66).

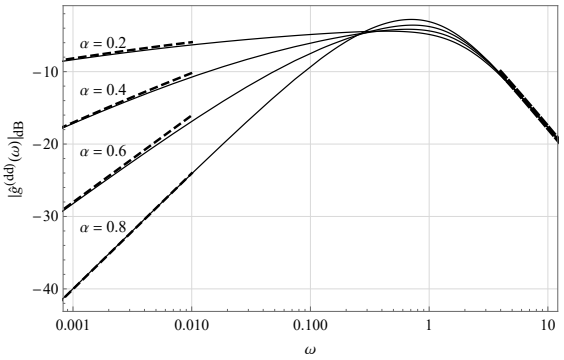

(a) Modulus of the transfer function $\hat{g}^{(\mathrm{dd})}$.

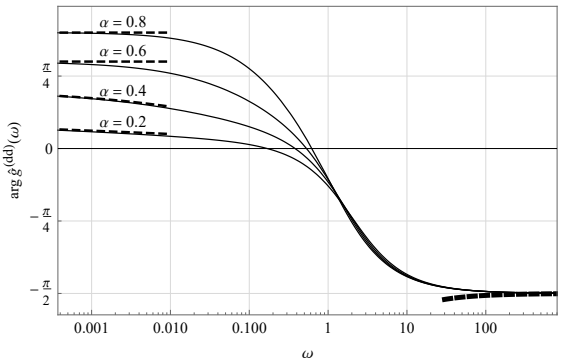

(b) Argument of the transfer function $\hat{g}^{(\mathrm{dd})}$.

Figure 6: Comparison of frequency characteristics of transfer function modulus and argument (solid line) with their asymptotics (dashed line) for dissipative-dissipative RLC circuit, obtained for model parameters: $\beta = 0.2$, $\tau_C = 0.1$, $\tau_\alpha = 2.5$, $\tau_L = 0.75$, and $\tau_\beta = 0.25$.

Note that the leading term in the low frequency asymptotics of the transfer function modulus (60) provides the possibility of determining the model parameters α and τ_α, since they respectively represent the slope and intercept of the function linear in $\log \omega$, while the leading term of the high frequency asymptotics (65) yields τ_L as the intercept of the linear function in $\log \omega$. Further, by considering the logarithm of the absolute value of transfer function argument's cotangent, see the first term in high frequency asymptotics (66), one determines the remaining model parameters β and τ_β, since

$$\log \left| \cot \arg \hat{g}^{(\mathrm{dd})}(\omega) \right| \sim (-1+\beta) \log \omega + \log \left(\frac{\tau_\beta}{\tau_L} \cos \frac{\beta \pi}{2} \right) \quad \text{as} \quad \omega \to \infty.$$

4.2 Generative-generative fractional RLC circuit

The real and imaginary parts of the equivalent impedance $Z_e^{(\mathrm{gg})}$, given by (40) and corresponding to the generative-generative fractional RLC circuit, rewritten in terms of classical and fractional time constants read

$$\mathrm{Re}\, Z_e^{(\mathrm{gg})}(\omega) = R \left(1 - \frac{\sin \frac{\mu \pi}{2}}{\tau_\mu \omega^{1+\mu}} - \tau_L \tau_\nu \omega^{1+\nu} \frac{\tau_L \sin \frac{\nu \pi}{2}}{\tau_\nu^2 \omega^{2\nu} + 2 \tau_L \tau_\nu \omega^\nu \cos \frac{\nu \pi}{2} + \tau_L^2} \right), \tag{67}$$

$$\mathrm{Im}\, Z_e^{(\mathrm{gg})}(\omega) = -R \left(\frac{1}{\tau_C \omega} + \frac{\cos \frac{\mu \pi}{2}}{\tau_\mu \omega^{1+\mu}} - \tau_L \tau_\nu \omega^{1+\nu} \frac{\tau_\nu \omega^\nu + \tau_L \cos \frac{\nu \pi}{2}}{\tau_\nu^2 \omega^{2\nu} + 2 \tau_L \tau_\nu \omega^\nu \cos \frac{\nu \pi}{2} + \tau_L^2} \right), \tag{68}$$

yielding the transfer function modulus and argument according to (55).

The frequency characteristics of transfer function modulus and argument, presented in Figure 7 and obtained for the same model parameters as in the case of plots from Figure 2, illustrate the possibility that the transfer function modulus has a vertical asymptote, while the argument abruptly changes by π, see the solid-line plots from Figures 7a and 7b, which is the property of transfer function having purely imaginary poles, that is exactly the case for the selected set of model parameters. In addition to non-integer zeros of the transfer function - its modulus tends to negative infinity as the frequency tends to zero, see also the form of transfer function $\hat{g}^{(\mathrm{gg})}$ given by (20) - the occurrence of a maximum followed by modulus' tendency to negative infinity as the frequency tends to infinity, see dashed- and dot-dashed-line plots from Figure 7a, is a consequence of the existence of complex conjugated poles of the transfer function, as it is the case for the selected sets of model parameters.

The transfer function argument in the case of dashed-line plot from Figure 7b decreases, which underlines the similarity with the integer order case, since the complex conjugated poles for selected model parameters have negative real part, contrary to the case of transfer function argument represented by dot-dashed line, that actually increases over π, although in Figure 7b drops by 2π due to the codomain of arcus tangent function being $(-\pi, \pi]$, again underlining the similarity with the integer order case, since the complex conjugated poles for this set of model parameters have positive real part.

Again, the transfer function argument illustrates the transition from the capacitive to inductive character of the circuit with the increase of the angular frequency, as well as its energy consumption/production properties, that in the case of solid- and dashed-line plots change with frequency from generative to dissipative, since the argument drops below $\frac{\pi}{2}$, and again to generative when the argument further drops below $-\frac{\pi}{2}$, while for the dot-dashed-line plot circuit's character is generative for the whole frequency range, since the argument has values either higher than $\frac{\pi}{2}$, or lower than $-\frac{\pi}{2}$ in the whole frequency range.

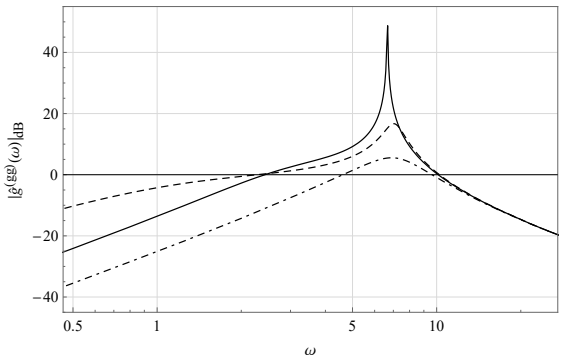

(a) Modulus of the transfer function $\hat{g}^{(\mathrm{gg})}$.

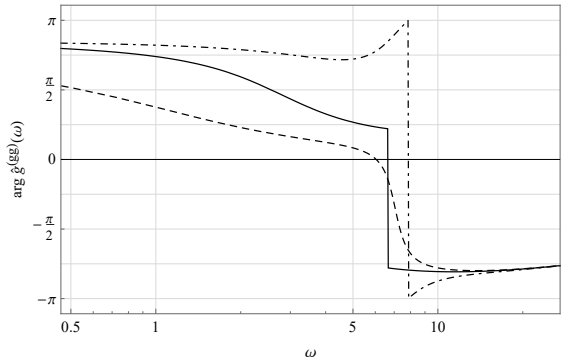

(b) Argument of the transfer function $\hat{g}^{(\mathrm{gg})}$.

Figure 7: Frequency characteristics of transfer function modulus and argument for generative-generative RLC circuit, obtained for model parameters: $\mu = 0.7$, $\nu = 0.9$, $\tau_C = 0.75$, $\tau_L = 0.75$, $\tau_\nu = 0.025$, and $\tau_\mu = 2.5$ - dot-dashed line, $\tau_\mu = 0.20980\ldots$ - solid line, and $\tau_\mu = 0.055$ - dashed line.

As for the dissipative-dissipative fractional RLC circuit, the capacitive character is dominant for low frequencies, so that the asymptotics of expressions (67) and (68), corresponding to $\mathrm{Re}\, Z_e^{(\mathrm{gg})}$ and $\mathrm{Im}\, Z_e^{(\mathrm{gg})}$, takes the following forms

$$\mathrm{Re}\, Z_e^{(\mathrm{gg})}(\omega) = -R\,\frac{\sin\frac{\mu\pi}{2}}{\tau_\mu\omega^{1+\mu}}\left(1 - \frac{\tau_\mu\omega^{1+\mu}}{\sin\frac{\mu\pi}{2}} + O(\omega^{2+\mu})\right), \quad \text{as} \quad \omega \to 0, \tag{69}$$

$$\mathrm{Im}\, Z_e^{(\mathrm{gg})}(\omega) = -R\,\frac{\cos\frac{\mu\pi}{2}}{\tau_\mu\omega^{1+\mu}}\left(1 + \frac{\tau_\mu\omega^{\mu}}{\tau_C\cos\frac{\mu\pi}{2}} + O(\omega^{2+\mu})\right), \quad \text{as} \quad \omega \to 0, \tag{70}$$

since the leading terms of real and imaginary parts of generative inductor's impedance $\frac{1}{Y_L^{(\mathrm{g})}}$, given by (32), are

$$\mathrm{Re}\,\frac{1}{Y_L^{(\mathrm{g})}} \sim -R\,\tau_\nu\omega^{1+\nu}\sin\frac{\nu\pi}{2} \quad \text{and} \quad \mathrm{Im}\,\frac{1}{Y_L^{(\mathrm{g})}} \sim R\,\tau_\nu\omega^{1+\nu}\cos\frac{\nu\pi}{2} \quad \text{as} \quad \omega \to 0, \tag{71}$$

so that the low frequency asymptotics of transfer function modulus, by $(55)_1$, (69), and (70), reads

$$\left|\hat{g}^{(\mathrm{gg})}(\omega)\right|_{\mathrm{dB}} = 20\log\left(\tau_\mu\omega^{1+\mu}\right) - 10\log\left(1 + 2\frac{\tau_\mu}{\tau_C}\omega^{\mu}\cos\frac{\mu\pi}{2} + \frac{\tau_\mu^2}{\tau_C^2}\omega^{2\mu} - 2\tau_\mu\omega^{1+\mu}\sin\frac{\mu\pi}{2} + O(\omega^{2+\mu})\right), \tag{72}$$

as $\omega \to 0$, while the transfer function argument, by $(55)_2$, (69), and (70), is

$$\cot\arg\hat{g}^{(\mathrm{gg})}(\omega) = -\tan\frac{\mu\pi}{2}\left(1 - \frac{\tau_\mu\omega^{\mu}}{\tau_C\cos\frac{\mu\pi}{2}} + \frac{\tau_\mu^2\omega^{2\mu}}{\tau_C^2\cos^2\frac{\mu\pi}{2}} - \frac{\tau_\mu^3\omega^{3\mu}}{\tau_C^3\cos^3\frac{\mu\pi}{2}}\right.$$

$$+\begin{cases} O(\omega^{4\mu}), & \text{if } \mu \in \left(0, \frac{1}{3}\right], \\ -\frac{\tau_\mu \omega^{1+\mu}}{\sin\frac{\mu\pi}{2}} + O(\omega^{4\mu}), & \text{if } \mu \in \left(\frac{1}{3}, \frac{1}{2}\right], \\ -\frac{\tau_\mu \omega^{1+\mu}}{\sin\frac{\mu\pi}{2}} + \frac{\tau_\mu^2 \omega^{1+2\mu}}{\tau_C \sin\frac{\mu\pi}{2}\cos\frac{\mu\pi}{2}} + O(\omega^{4\mu}), & \text{if } \mu \in \left(\frac{1}{2}, \frac{2}{3}\right], \\ -\frac{\tau_\mu \omega^{1+\mu}}{\sin\frac{\mu\pi}{2}} + \frac{\tau_\mu^2 \omega^{1+2\mu}}{\tau_C \sin\frac{\mu\pi}{2}\cos\frac{\mu\pi}{2}} + O(\omega^{2+\mu}), & \text{if } \mu \in \left(\frac{2}{3}, 1\right), \end{cases} \Bigg) \tag{73}$$

as $\omega \to 0$, since

$$\cot\arg \hat{g}^{(\mathrm{gg})}(\omega) = -\tan\frac{\mu\pi}{2}\left(1 - \frac{\tau_\mu \omega^{1+\mu}}{\sin\frac{\mu\pi}{2}} + O(\omega^{2+\mu})\right) \times \left(1 - \frac{\tau_\mu \omega^{\mu}}{\tau_C \cos\frac{\mu\pi}{2}} + \frac{\tau_\mu^2 \omega^{2\mu}}{\tau_C^2 \cos^2\frac{\mu\pi}{2}} - \frac{\tau_\mu^3 \omega^{3\mu}}{\tau_C^3 \cos^3\frac{\mu\pi}{2}} + \begin{cases} O(\omega^{4\mu}), & \text{if } \mu \in \left(0, \frac{2}{3}\right], \\ O(\omega^{2+\mu}), & \text{if } \mu \in \left(\frac{2}{3}, 1\right), \end{cases}\right)$$

due to the series expansion $\frac{1}{1+x} = 1 - x + x^2 - x^3 + O(x^4)$ as $x \to 0$.

Generative-generative fractional RLC circuit displays inductive properties for high frequencies as already noted, see $(43)_2$ and $(44)_2$, therefore the corresponding asymptotics of $\operatorname{Re} Z_e^{(\mathrm{gg})}$ and $\operatorname{Im} Z_e^{(\mathrm{gg})}$, given by (67) and (68), reads

$$\operatorname{Re} Z_e^{(\mathrm{gg})}(\omega) = -R\frac{\tau_L^2}{\tau_\nu}\omega^{1-\nu}\sin\frac{\nu\pi}{2}\left(1 - 2\frac{\tau_L}{\tau_\nu}\omega^{-\nu}\cos\frac{\nu\pi}{2} + \begin{cases} O(\omega^{-2\nu}), & \text{if } \nu \in \left(0, \frac{1}{3}\right], \\ -\frac{\tau_L \omega^{-1+\nu}}{\tau_L^2 \sin\frac{\nu\pi}{2}} + O(\omega^{-2\nu}), & \text{if } \nu \in \left(\frac{1}{3}, 1\right), \end{cases}\right) \tag{74}$$

$$\operatorname{Im} Z_e^{(\mathrm{gg})}(\omega) = R\tau_L\omega\left(1 - \frac{\tau_L}{\tau_\nu}\omega^{-\nu}\cos\frac{\nu\pi}{2} - \frac{\tau_L^2}{\tau_\nu^2}\omega^{-2\nu}\left(1 - 2\cos^2\frac{\nu\pi}{2}\right) + O(\omega^{-3\nu})\right), \tag{75}$$

as $\omega \to \infty$, since for the generative inductor, according to (32), the high frequency asymptotics of $\operatorname{Re}\frac{1}{Y_L^{(\mathrm{g})}}$ is

$$\begin{aligned} \operatorname{Re}\frac{1}{Y_L^{(\mathrm{g})}}(\omega) &= -R\frac{\tau_L^2}{\tau_\nu}\omega^{1-\nu}\sin\frac{\nu\pi}{2}\frac{1}{1 + 2\frac{\tau_L}{\tau_\nu}\omega^{-\nu}\cos\frac{\nu\pi}{2} + \frac{\tau_L^2}{\tau_\nu^2}\omega^{-2\nu}} \\ &= -R\frac{\tau_L^2}{\tau_\nu}\omega^{1-\nu}\sin\frac{\nu\pi}{2}\left(1 - 2\frac{\tau_L}{\tau_\nu}\omega^{-\nu}\cos\frac{\nu\pi}{2} + O(\omega^{-2\nu})\right), \end{aligned} \tag{76}$$

due to the series expansion $\frac{1}{1+x} = 1 - x + O(x^2)$ as $x \to 0$, while according to (32), the high frequency asymptotics of $\operatorname{Im}\frac{1}{Y_L^{(\mathrm{g})}}$ is

$$\begin{aligned} \operatorname{Im}\frac{1}{Y_L^{(\mathrm{g})}}(\omega) &= R\tau_L\omega\frac{1 + \frac{\tau_L}{\tau_\nu}\omega^{-\nu}\cos\frac{\nu\pi}{2}}{1 + 2\frac{\tau_L}{\tau_\nu}\omega^{-\nu}\cos\frac{\nu\pi}{2} + \frac{\tau_L^2}{\tau_\nu^2}\omega^{-2\nu}} \\ &= R\tau_L\omega\left(1 + \frac{\tau_L}{\tau_\nu}\omega^{-\nu}\cos\frac{\nu\pi}{2}\right)\left(1 - 2\frac{\tau_L}{\tau_\nu}\omega^{-\nu}\cos\frac{\nu\pi}{2} - \frac{\tau_L^2}{\tau_\nu^2}\omega^{-2\nu}\left(1 - 4\cos^2\frac{\nu\pi}{2}\right) + O(\omega^{-3\nu})\right) \\ &= R\tau_L\omega\left(1 - \frac{\tau_L}{\tau_\nu}\omega^{-\nu}\cos\frac{\nu\pi}{2} - \frac{\tau_L^2}{\tau_\nu^2}\omega^{-2\nu}\left(1 - 2\cos^2\frac{\nu\pi}{2}\right) + O(\omega^{-3\nu})\right), \end{aligned} \tag{77}$$

due to the series expansion $\frac{1}{1+x} = 1 - x + x^2 + O(x^3)$ as $x \to 0$, taking into account that the leading terms of generative capacitor's impedance (31) are

$$\operatorname{Re} Z_C^{(\mathrm{g})} \sim -R\frac{1}{\tau_\mu}\omega^{-1-\mu}\sin\frac{\mu\pi}{2} \quad \text{and} \quad \operatorname{Im} Z_C^{(\mathrm{g})} \sim -R\frac{1}{\tau_C}\omega^{-1}, \quad \text{as} \quad \omega \to \infty, \tag{78}$$

so that (74) and (75), by (55), yield the high frequency asymptotics of transfer function modulus and argument in the respective forms

$$\left|\hat{g}^{(\mathrm{gg})}(\omega)\right|_{\mathrm{dB}} = -20\log(\tau_L\omega) - 10\log\left(1 - 2\frac{\tau_L}{\tau_\nu}\omega^{-\nu}\cos\frac{\nu\pi}{2} - \frac{\tau_L^2}{\tau_\nu^2}\omega^{-2\nu}\left(1 - 4\cos^2\frac{\nu\pi}{2}\right) + \begin{cases} O(\omega^{-3\nu}), & \text{if } \nu \in \left(0, \frac{1}{2}\right], \\ -2\frac{1}{\tau_\nu}\omega^{-1-\nu}\sin\frac{\nu\pi}{2} + O(\omega^{-3\nu}), & \text{if } \nu \in \left(\frac{1}{2}, \frac{2}{3}\right], \\ -2\frac{1}{\tau_\nu}\omega^{-1-\nu}\sin\frac{\nu\pi}{2} + \frac{1}{\tau_L^2}\omega^{-2} + O(\omega^{-3\nu}), & \text{if } \nu \in \left(\frac{2}{3}, 1\right), \end{cases}\right), \tag{79}$$

$$\cot\arg\hat{g}^{(\mathrm{gg})}(\omega)=\frac{\tau_L}{\tau_\nu}\omega^{-\nu}\sin\frac{\nu\pi}{2}\left(1-\frac{\tau_L}{\tau_\nu}\omega^{-\nu}\cos\frac{\nu\pi}{2}\right.$$
$$\left.+\begin{cases}O(\omega^{-2\nu}), & \text{if } \nu\in\left(0,\frac{1}{3}\right],\\ -\frac{\omega^{-1+\nu}}{\tau_\nu\sin\frac{\nu\pi}{2}}+O(\omega^{-2\nu}), & \text{if } \nu\in\left(\frac{1}{3},\frac{1}{2}\right],\\ -\frac{\omega^{-1+\nu}}{\tau_\nu\sin\frac{\nu\pi}{2}}-\frac{1}{\tau_L}\omega^{-1}\cot\frac{\nu\pi}{2}+O(\omega^{-2\nu}), & \text{if } \nu\in\left(\frac{1}{2},1\right),\end{cases}\right) \tag{80}$$

as $\omega\to\infty$, since (74) and (75) used in $(55)_2$ yield

$$\cot\arg\hat{g}^{(\mathrm{gg})}(\omega)=\frac{\tau_L}{\tau_\nu}\omega^{-\nu}\sin\frac{\nu\pi}{2}\left(1-2\frac{\tau_L}{\tau_\nu}\omega^{-\nu}\cos\frac{\nu\pi}{2}+\begin{cases}O(\omega^{-2\nu}), & \text{if } \nu\in\left(0,\frac{1}{3}\right],\\ -\frac{\tau_\nu\omega^{-1+\nu}}{\tau_L^2\sin\frac{\nu\pi}{2}}+O(\omega^{-2\nu}), & \text{if } \nu\in\left(\frac{1}{3},1\right),\end{cases}\right)$$
$$\times\left(1+\frac{\tau_L}{\tau_\nu}\omega^{-\nu}\cos\frac{\nu\pi}{2}+\frac{\tau_L^2}{\tau_\nu^2}\omega^{-2\nu}\sin^2\frac{\nu\pi}{2}+O(\omega^{-3\nu})\right),$$

as $\omega\to\infty$, according to the series expansion $\frac{1}{1+x}=1-x+x^2+O(x^3)$ as $x\to 0$.

Figure 8 presents the plots of transfer function modulus and argument versus the angular frequency for different values of fractional order of generative capacitor, together with their asymptotics. According to the low frequency asymptotics (72), the transfer function modulus is a linear function of $\log\omega$, with the slope and intercept respectively determined by the model parameters μ and τ_μ, see also Figure 8a, while the low frequency asymptotics of transfer function argument (73) implies the dependence on the parameter μ, as obvious from Figure 8b. On the other hand, the high frequency asymptotics of transfer function modulus (79) yields τ_L as the intercept of the linear function in $\log\omega$, see Figure 8a, while the remaining model parameters ν and τ_ν are determined by the logarithm of the absolute value of transfer function argument's cotangent for high frequencies, see the asymptotics (80) and agreement between the asymptotic curve and the frequency characteristics in Figure 8b.

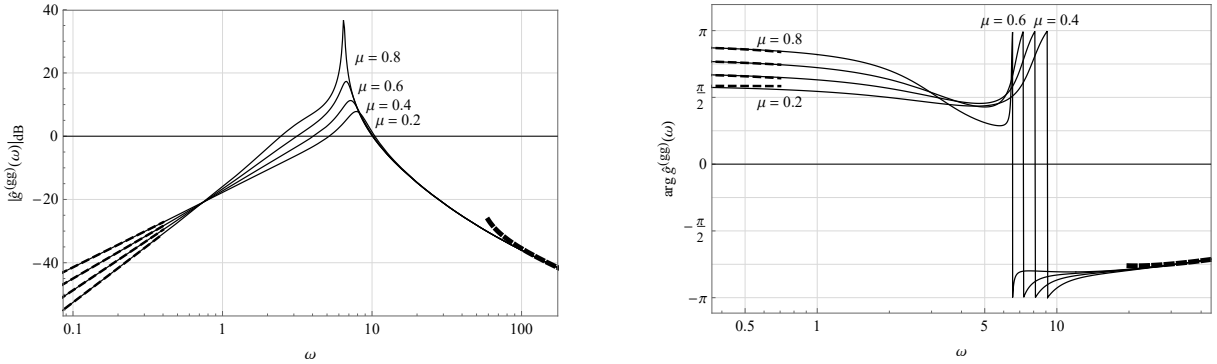

(a) Modulus of the transfer function $\hat{g}^{(\mathrm{gg})}$.

(b) Argument of the transfer function $\hat{g}^{(\mathrm{gg})}$.

Figure 8: Comparison of frequency characteristics of transfer function modulus and argument (solid line) with their asymptotics (dashed line) for generative-generative RLC circuit, obtained for model parameters: $\nu=0.9$, $\tau_C=0.75$, $\tau_\mu=0.15$, $\tau_L=0.75$, and $\tau_\nu=0.025$.

4.3 Dissipative-generative fractional RLC circuit

Rewriting the real and imaginary parts of the equivalent impedance $Z_e^{(\mathrm{dg})}$, given by $(45)_1$, of the dissipative-generative fractional RLC circuit using classical and fractional time constants yields

$$\mathrm{Re}\,Z_e^{(\mathrm{dg})}(\omega)=R\left(1+\frac{\tau_\alpha\omega^\alpha\cos\frac{\alpha\pi}{2}}{\tau_C^2\omega^2+2\tau_C\tau_\alpha\omega^{1+\alpha}\sin\frac{\alpha\pi}{2}+\tau_\alpha^2\omega^{2\alpha}}-\tau_L\tau_\nu\omega^{1+\nu}\frac{\tau_L\sin\frac{\nu\pi}{2}}{\tau_\nu^2\omega^{2\nu}+2\tau_L\tau_\nu\omega^\nu\cos\frac{\nu\pi}{2}+\tau_L^2}\right), \tag{81}$$

$$\mathrm{Im}\,Z_e^{(\mathrm{dg})}(\omega)=-R\left(\frac{\tau_C\omega+\tau_\alpha\omega^\alpha\sin\frac{\alpha\pi}{2}}{\tau_C^2\omega^2+2\tau_C\tau_\alpha\omega^{1+\alpha}\sin\frac{\alpha\pi}{2}+\tau_\alpha^2\omega^{2\alpha}}-\tau_L\tau_\nu\omega^{1+\nu}\frac{\tau_\nu\omega^\nu+\tau_L\cos\frac{\nu\pi}{2}}{\tau_\nu^2\omega^{2\nu}+2\tau_L\tau_\nu\omega^\nu\cos\frac{\nu\pi}{2}+\tau_L^2}\right), \tag{82}$$

giving the transfer function modulus and argument according to (55).

Figure 9 presents the Bode diagrams of transfer function modulus and argument, obtained for the same set of model parameters as the plots in Figure 3, corresponding to the band-pass filter. The transfer function $\hat{g}^{(\mathrm{dg})}$ given by (23) has a non-integer zero at the origin, that can be recognized from the plots of transfer function modulus from Figure 9a, as well as complex conjugated poles, obtained as a consequence of the chosen sets of model parameters, either with nonzero real part, that correspond to the plots of transfer function modulus depicted by dot-dashed and dashed lines, or purely imaginary ones, corresponding to the solid-line plot. Plots of the transfer function argument versus the angular frequency support the statement regarding the type of poles and their real part, since if poles have nonzero real part, the argument decreases if pole's real part is obtained to be negative and increases over π if pole's real part is obtained to be positive, while in the case of purely imaginary poles, the value of argument drops by π.

Clearly, the fractional RLC circuit is dissipative for relatively low frequencies, since arguments' values belong to interval $(-\frac{\pi}{2}, \frac{\pi}{2})$, and eventually becomes generative: abruptly for the model parameters corresponding to the solid-line plot when the circuit simultaneously becomes of inductive type as well, since the argument drops below $-\frac{\pi}{2}$, and gradually either for mid-range frequencies in the case of dashed-line plots, or for high frequencies in the case of dot-dashed-line plots.

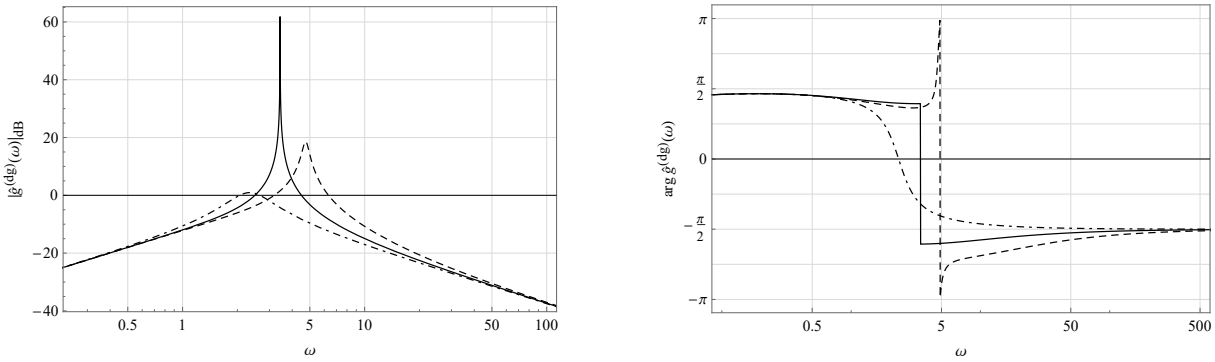

(a) Modulus of the transfer function $\hat{g}^{(\mathrm{dg})}$.

(b) Argument of the transfer function $\hat{g}^{(\mathrm{dg})}$.

Figure 9: Frequency characteristics of transfer function modulus and argument for dissipative-generative RLC circuit, obtained for model parameters: $\alpha = 0.25$, $\nu = 0.85$, $\tau_C = 0.25$, $\tau_\alpha = 0.005$, $\tau_L = 0.75$, and $\tau_\nu = 5$ - dot-dashed line, $\tau_\nu = 0.23329\ldots$ - solid line, and $\tau_\nu = 0.09$ - dashed line.

Although the dissipative-generative RLC circuit contains dissipative capacitor so as the dissipative-dissipative circuit, due to the different orders of the leading terms corresponding to the generative and dissipative inductor, compare (71) with (30), the low frequency asymptotics of real and imaginary parts of dissipative capacitor's impedance $\mathrm{Re}\,\frac{1}{Y_C^{(\mathrm{d})}}$ and $\mathrm{Im}\,\frac{1}{Y_C^{(\mathrm{d})}}$, according to (29), is calculated as

$$\begin{aligned}
\mathrm{Re}\,\frac{1}{Y_C^{(\mathrm{d})}(\omega)} &= R\frac{\cos\frac{\alpha\pi}{2}}{\tau_\alpha\omega^\alpha}\,\frac{1}{1+2\frac{\tau_C}{\tau_\alpha}\omega^{1-\alpha}\sin\frac{\alpha\pi}{2}+\frac{\tau_C^2}{\tau_\alpha^2}\omega^{2-2\alpha}} \\
&= R\frac{\cos\frac{\alpha\pi}{2}}{\tau_\alpha\omega^\alpha}\left(1-2\frac{\tau_C}{\tau_\alpha}\omega^{1-\alpha}\sin\frac{\alpha\pi}{2}+O(\omega^{2-2\alpha})\right), \quad \text{as} \quad \omega\to 0, \\
\mathrm{Im}\,\frac{1}{Y_C^{(\mathrm{d})}(\omega)} &= -R\frac{\sin\frac{\alpha\pi}{2}}{\tau_\alpha\omega^\alpha}\,\frac{1+\frac{\tau_C}{\tau_\alpha}\omega^{1-\alpha}\frac{1}{\sin\frac{\alpha\pi}{2}}}{1+2\frac{\tau_C}{\tau_\alpha}\omega^{1-\alpha}\sin\frac{\alpha\pi}{2}+\frac{\tau_C^2}{\tau_\alpha^2}\omega^{2-2\alpha}} \\
&= -R\frac{\sin\frac{\alpha\pi}{2}}{\tau_\alpha\omega^\alpha}\left(1-2\frac{\tau_C}{\tau_\alpha}\omega^{1-\alpha}\sin\frac{\alpha\pi}{2}\left(1-\frac{1}{2\sin^2\frac{\alpha\pi}{2}}\right)+O(\omega^{2-2\alpha})\right), \quad \text{as} \quad \omega\to 0,
\end{aligned}$$

by the series expansion $\frac{1}{1+x} = 1 - x + O(x^2)$, as $x \to 0$, transforming the real and imaginary parts of circuit's equivalent impedance $\mathrm{Re}\,Z_e^{(\mathrm{dg})}$ and $\mathrm{Im}\,Z_e^{(\mathrm{dg})}$, given by (81) and (82), into

$$\mathrm{Re}\,Z_e^{(\mathrm{dg})}(\omega) = R\,\frac{\cos\frac{\alpha\pi}{2}}{\tau_\alpha\omega^\alpha}\left(1-2\frac{\tau_C}{\tau_\alpha}\omega^{1-\alpha}\sin\frac{\alpha\pi}{2}+\begin{cases}\frac{\tau_\alpha\omega^\alpha}{\cos\frac{\alpha\pi}{2}}+O(\omega^{2-2\alpha}), & \text{if } \alpha\in\left(0,\frac{2}{3}\right),\\ O(\omega^{2-2\alpha}), & \text{if } \alpha\in\left[\frac{2}{3},1\right),\end{cases}\right) \tag{83}$$

$$\operatorname{Im} Z_e^{(\mathrm{dg})}(\omega) = -R\,\frac{\sin\frac{\alpha\pi}{2}}{\tau_\alpha\omega^\alpha}\left(1 - 2\frac{\tau_C}{\tau_\alpha}\omega^{1-\alpha}\sin\frac{\alpha\pi}{2}\left(1 - \frac{1}{2\sin^2\frac{\alpha\pi}{2}}\right) + O(\omega^{2-2\alpha})\right), \tag{84}$$

as $\omega \to 0$, so that, by $(55)_1$, (83), and (84), for the transfer function modulus one has

$$\left|\hat{g}^{(\mathrm{dg})}(\omega)\right|_{\mathrm{dB}} = 20\log(\tau_\alpha\omega^\alpha) - 10\log\left(1 - 2\frac{\tau_C}{\tau_\alpha}\omega^{1-\alpha}\sin\frac{\alpha\pi}{2}\right.$$
$$\left. + \begin{cases} 2\tau_\alpha\omega^\alpha\cos\frac{\alpha\pi}{2} + \tau_\alpha^2\omega^{2\alpha} - 4\tau_C\omega\sin\frac{\alpha\pi}{2}\cos\frac{\alpha\pi}{2} + O(\omega^{2-2\alpha}), & \text{if } \alpha \in \left(0, \frac{1}{2}\right), \\ 2\tau_\alpha\omega^\alpha\cos\frac{\alpha\pi}{2} + O(\omega^{2-2\alpha}), & \text{if } \alpha \in \left[\frac{1}{2}, \frac{2}{3}\right), \\ O(\omega^{2-2\alpha}), & \text{if } \alpha \in \left[\frac{2}{3}, 1\right), \end{cases}\right) \tag{85}$$

as $\omega \to 0$, while the transfer function argument, by $(55)_2$, (83), and (84), is

$$\cot\arg\hat{g}^{(\mathrm{dg})}(\omega) = \cot\frac{\alpha\pi}{2}\left(1 - \frac{\tau_C}{\tau_\alpha}\omega^{1-\alpha}\frac{1}{\sin\frac{\alpha\pi}{2}}\right.$$
$$\left. + \begin{cases} \frac{\tau_\alpha\omega^\alpha}{\cos\frac{\alpha\pi}{2}} + 2\tau_C\omega\tan\frac{\alpha\pi}{2}\left(1 - \frac{1}{2\sin^2\frac{\alpha\pi}{2}}\right) + O(\omega^{2-2\alpha}), & \text{if } \alpha \in \left(0, \frac{1}{2}\right), \\ \frac{\tau_\alpha\omega^\alpha}{\cos\frac{\alpha\pi}{2}} + O(\omega^{2-2\alpha}), & \text{if } \alpha \in \left[\frac{1}{2}, \frac{2}{3}\right), \\ O(\omega^{2-2\alpha}), & \text{if } \alpha \in \left[\frac{2}{3}, 1\right), \end{cases}\right) \tag{86}$$

as $\omega \to 0$, since

$$\cot\arg\hat{g}^{(\mathrm{dg})}(\omega) = \cot\frac{\alpha\pi}{2}\left(1 - 2\frac{\tau_C}{\tau_\alpha}\omega^{1-\alpha}\sin\frac{\alpha\pi}{2} + \begin{cases} \frac{\tau_\alpha\omega^\alpha}{\cos\frac{\alpha\pi}{2}} + O(\omega^{2-2\alpha}), & \text{if } \alpha \in \left(0, \frac{2}{3}\right), \\ O(\omega^{2-2\alpha}), & \text{if } \alpha \in \left[\frac{2}{3}, 1\right), \end{cases}\right)$$
$$\times\left(1 + 2\frac{\tau_C}{\tau_\alpha}\omega^{1-\alpha}\sin\frac{\alpha\pi}{2}\left(1 - \frac{1}{2\sin^2\frac{\alpha\pi}{2}}\right) + O(\omega^{2-2\alpha})\right) \quad \text{as} \quad \omega \to 0,$$

according to $\frac{1}{1+x} = 1 - x + O(x^2)$, as $x \to 0$.

In the case of dissipative-generative fractional RLC circuit, as for all previously considered circuits, the inductive properties are dominant for high frequencies and therefore one uses already calculated asymptotics (76) and (77) of the real and imaginary parts of generative inductor's impedance $\frac{1}{Y_L^{(\mathrm{g})}}$, given by (32), since the upper limits of orders of leading terms of dissipative and generative capacitors' impedances are equal, compare (64) with (78), which implies that the high frequency asymptotics of the real and imaginary parts of circuit's equivalent impedance $\operatorname{Re} Z_e^{(\mathrm{dg})}$ and $\operatorname{Im} Z_e^{(\mathrm{dg})}$ are the same as the real and imaginary parts of equivalent impedance of the generative-generative circuit $\operatorname{Re} Z_e^{(\mathrm{gg})}$ and $\operatorname{Im} Z_e^{(\mathrm{gg})}$, i.e., $\operatorname{Re} Z_e^{(\mathrm{dg})} = \operatorname{Re} Z_e^{(\mathrm{gg})}$ and $\operatorname{Im} Z_e^{(\mathrm{dg})} = \operatorname{Im} Z_e^{(\mathrm{gg})}$ as $\omega \to \infty$, thus being given by (74) and (75), yielding the transfer function modulus and argument in the same forms as for the generative-generative circuit, i.e., given by the expression (79) for the transfer function modulus and (80) for the transfer function argument.

Frequency characteristics of transfer function modulus and argument, together with their asymptotics, are presented in Figure 10. The discussion about the low frequency asymtotic behavior of the dissipative-generative RLC circuit is the same as for the dissipative-dissipative RLC circuit, since the capacitive character of circuit prevails, compare also the leading terms in the low frequency asymptotics of transfer function modulus and argument (60) with (85) and (61) with (86), respectively. On the other hand, the discussion about the high frequency asymtotic behavior of the dissipative-generative circuit is the same as for the generative-generative circuit, since the inductive character of circuit prevails, see the leading terms in the high frequency asymptotics of transfer function modulus and argument (79) and (80).

4.4 Generative-dissipative fractional RLC circuit

Equivalent impedance $Z_e^{(\mathrm{gd})}$ of the generative-dissipative fractional RLC circuit, given by $(45)_2$, implies

$$\operatorname{Re} Z_e^{(\mathrm{gd})}(\omega) = R\left(1 - \frac{\sin\frac{\mu\pi}{2}}{\tau_\mu\omega^{1+\mu}} + \tau_\beta\omega^\beta\cos\frac{\beta\pi}{2}\right), \tag{87}$$

$$\operatorname{Im} Z_e^{(\mathrm{gd})}(\omega) = -R\left(\frac{1}{\tau_C\omega} + \frac{\cos\frac{\mu\pi}{2}}{\tau_\mu\omega^{1+\mu}} - \tau_L\omega - \tau_\beta\omega^\beta\sin\frac{\beta\pi}{2}\right), \tag{88}$$

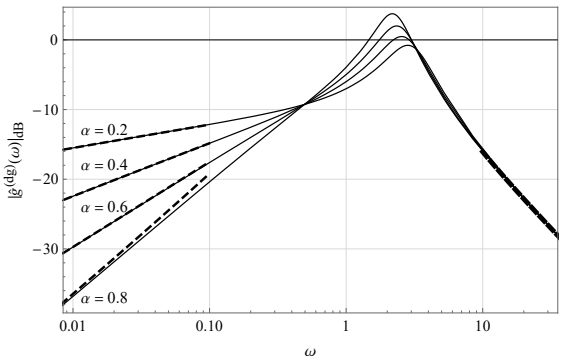

(a) Modulus of the transfer function $\hat{g}^{(\mathrm{dg})}$.

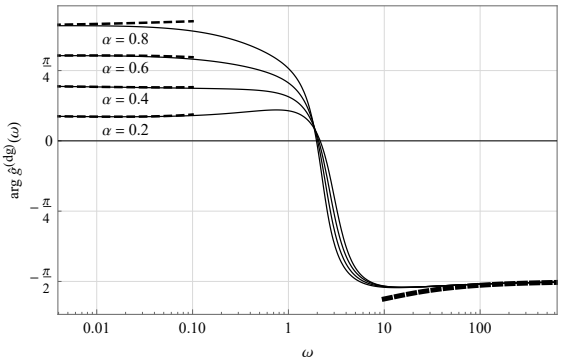

(b) Argument of the transfer function $\hat{g}^{(\mathrm{dg})}$.

Figure 10: Comparison of frequency characteristics of transfer function modulus and argument (solid line) with their asymptotics (dashed line) for dissipative-generative *RLC* circuit, obtained for model parameters: $\nu = 0.75$, $\tau_C = 0.2$, $\tau_\alpha = 0.5$, $\tau_L = 0.75$, and $\tau_\nu = 0.5$.

when its real and imaginary parts are rewritten in terms of classical and fractional time constants, yielding the transfer function modulus and argument according to (55).

Frequency characteristics of transfer function modulus and argument corresponding to the generative-dissipative *RLC* circuit, presented in Figure 11 and obtained for the same set of model parameters as the plots in Figure 4, are of the same shape as the frequency characteristics corresponding to the dissipative-generative circuit, see Figure 9, since the transfer function $\hat{g}^{(\mathrm{gd})}$, given by (24), for selected sets of model parameters also has either complex conjugated poles with positive or negative real parts, or purely imaginary poles.

Although, the plots of transfer function argument from Figure 11b are qualitatively the same as the ones from Figure 9b, they quantitatively correspond to the generative circuit for relatively low frequencies, since arguments' values are above $\frac{\pi}{2}$, while the circuit eventually becomes dissipative: abruptly for the model parameters corresponding to the solid-line plot when the circuit simultaneously becomes of inductive type as well, since the argument drops to interval $(-\frac{\pi}{2}, 0)$, and gradually either for mid-range frequencies in the case of dashed-line plots, or for high frequencies in the case of dot-dashed-line plots.

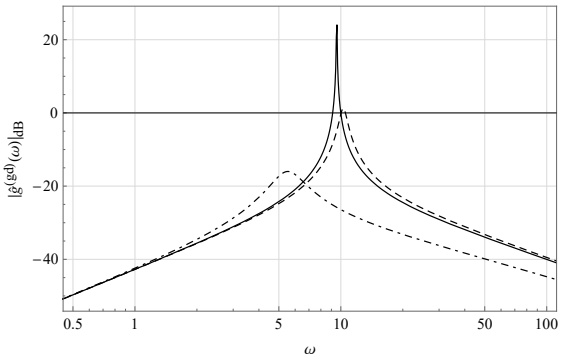

(a) Modulus of the transfer function $\hat{g}^{(\mathrm{gd})}$.

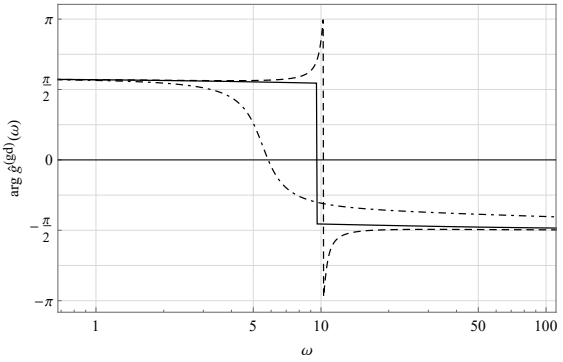

(b) Argument of the transfer function $\hat{g}^{(\mathrm{gd})}$.

Figure 11: Frequency characteristics of transfer function modulus and argument for generative-dissipative *RLC* circuit, obtained for model parameters: $\mu = 0.2$, $\beta = 0.6$, $\tau_C = 0.025$, $\tau_\mu = 0.01$, $\tau_L = 0.95$, and $\tau_\beta = 5.5$ - dot-dashed line, $\tau_\beta = 0.46607\ldots$ - solid line, and $\tau_\beta = 0.01$ - dashed line.

In the low frequency limit, the impedance $Z_C^{(\mathrm{g})}$ of dissipative capacitor, given by (31), dominates the equivalent impedance and therefore expressions (87) and (88) become

$$\mathrm{Re}\, Z_e^{(\mathrm{gd})}(\omega) = -R\, \frac{\sin\frac{\mu\pi}{2}}{\tau_\mu \omega^{1+\mu}} \left(1 - \frac{\tau_\mu \omega^{1+\mu}}{\sin\frac{\mu\pi}{2}} + O(\omega^{1+\mu+\delta})\right), \quad \text{as} \quad \omega \to 0, \tag{89}$$

$$\mathrm{Im}\, Z_e^{(\mathrm{gd})}(\omega) = -R\, \frac{\cos\frac{\mu\pi}{2}}{\tau_\mu \omega^{1+\mu}} \left(1 + \frac{\tau_\mu \omega^{\mu}}{\tau_C \cos\frac{\mu\pi}{2}} + O(\omega^{1+\mu+\delta})\right), \quad \text{as} \quad \omega \to 0, \tag{90}$$

where δ is chosen to be smaller than β, i.e., smaller than the order of the leading terms of the real and imaginary parts of dissipative inductor's impedance $\operatorname{Re} Z_L^{(\mathrm{d})}$ and $\operatorname{Im} Z_L^{(\mathrm{d})}$, see (30), implying by $(55)_1$, (89), and (90) the low frequency asymptotics of the transfer function modulus as

$$\left|\hat{g}^{(\mathrm{gd})}(\omega)\right|_{\mathrm{dB}} = 20\log\left(\tau_\mu\omega^{1+\mu}\right) - 10\log\left(1 + 2\frac{\tau_\mu}{\tau_C}\omega^\mu\cos\frac{\mu\pi}{2} + \frac{\tau_\mu^2}{\tau_C^2}\omega^{2\mu} - 2\tau_\mu\omega^{1+\mu}\sin\frac{\mu\pi}{2} + O(\omega^{1+\mu+\delta})\right), \tag{91}$$

as $\omega \to 0$, while the transfer function argument, by $(55)_2$, (89), and (90), is

$$\begin{aligned}\cot\arg\hat{g}^{(\mathrm{gd})}(\omega) = -\tan\frac{\mu\pi}{2}\Bigg(1 - \frac{\tau_\mu\omega^\mu}{\tau_C\cos\frac{\mu\pi}{2}} + \frac{\tau_\mu^2\omega^{2\mu}}{\tau_C^2\cos^2\frac{\mu\pi}{2}} \\ + \begin{cases} O(\omega^{3\mu}), & \text{if } \mu \in \left(0, \frac{1}{2}\right], \\ -\frac{\tau_\mu\omega^{1+\mu}}{\sin\frac{\mu\pi}{2}} + O(\omega^{3\mu}), & \text{if } \mu \in \left(\frac{1}{2}, \frac{1+\delta}{2}\right], \\ -\frac{\tau_\mu\omega^{1+\mu}}{\sin\frac{\mu\pi}{2}} + O(\omega^{1+\mu+\delta}), & \text{if } \mu \in \left(\frac{1+\delta}{2}, 1\right), \end{cases}\Bigg)\end{aligned} \tag{92}$$

as $\omega \to 0$, since

$$\begin{aligned}\cot\arg\hat{g}^{(\mathrm{gd})}(\omega) = -\tan\frac{\mu\pi}{2}\left(1 - \frac{\tau_\mu\omega^{1+\mu}}{\sin\frac{\mu\pi}{2}} + O(\omega^{1+\mu+\delta})\right) \\ \times\left(1 - \frac{\tau_\mu\omega^\mu}{\tau_C\cos\frac{\mu\pi}{2}} + \frac{\tau_\mu^2\omega^{2\mu}}{\tau_C^2\cos^2\frac{\mu\pi}{2}} + \begin{cases} O(\omega^{3\mu}), & \text{if } \mu \in \left(0, \frac{1+\delta}{2}\right], \\ O(\omega^{1+\mu+\delta}), & \text{if } \mu \in \left(\frac{1+\delta}{2}, 1\right). \end{cases}\right)\end{aligned}$$

In the case of generative-dissipative fractional RLC circuit, as for all previously considered circuits, the inductive properties are dominant for high frequencies and since the upper limits of orders of leading terms of generative and dissipative capacitors' impedances are equal, compare (78) with (64), the high frequency asymptotics of the real and imaginary parts of circuit's equivalent impedance $\operatorname{Re} Z_e^{(\mathrm{gd})}$ and $\operatorname{Im} Z_e^{(\mathrm{gd})}$ are the same as the real and imaginary parts of equivalent impedance of the dissipative-dissipative circuit $\operatorname{Re} Z_e^{(\mathrm{dd})}$ and $\operatorname{Im} Z_e^{(\mathrm{dd})}$, i.e., $\operatorname{Re} Z_e^{(\mathrm{gd})} = \operatorname{Re} Z_e^{(\mathrm{dd})}$ and $\operatorname{Im} Z_e^{(\mathrm{gd})} = \operatorname{Im} Z_e^{(\mathrm{dd})}$ as $\omega \to \infty$, and therefore given by (62) and (63), yielding the transfer function modulus and argument in the same forms as for the dissipative-dissipative circuit, i.e., given by the expression (65) for the transfer function modulus and (66) for the transfer function argument.

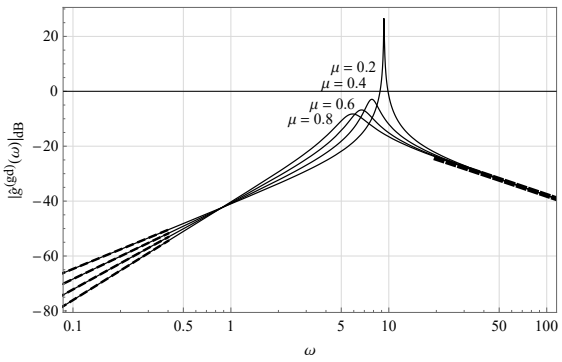

(a) Modulus of the transfer function $\hat{g}^{(\mathrm{gd})}$.

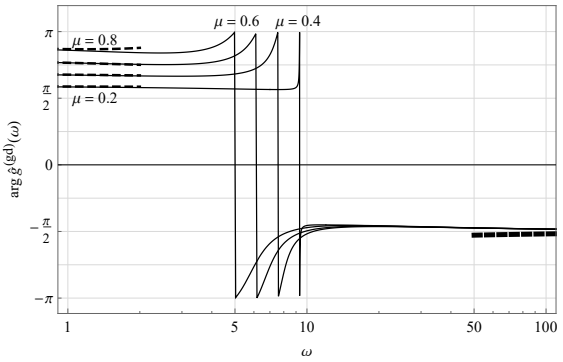

(b) Argument of the transfer function $\hat{g}^{(\mathrm{gd})}$.

Figure 12: Comparison of frequency characteristics of transfer function modulus and argument (solid line) with their asymptotics (dashed line) for generative-dissipative RLC circuit, obtained for model parameters: $\beta = 0.5$, $\tau_C = 0.07$, $\tau_\mu = 0.01$, $\tau_L = 0.75$, and $\tau_\beta = 0.5$.

Frequency characteristics of transfer function modulus and argument, together with their asymptotics, are presented in Figure 12. The discussion about the low frequency asymtotic behavior of the generative-dissipative RLC circuit is the same as for the generative-generative RLC circuit, since the capacitive character of circuit prevails, compare also the leading terms in the low frequency asymptotics of transfer function modulus and argument (72) with (91) and (73) with (92), respectively. On the other hand, the discussion about the high frequency asymtotic behavior of the generative-dissipative circuit is the same as for the dissipative-dissipative circuit, since the inductive character of circuit prevails, see the leading terms in the high frequency asymptotics of transfer function modulus and argument (65) and (66).

5 Conclusion

Constitutive equations of dissipative and generative capacitor (1) and (2), along with the constitutive models (3) and (4) corresponding to the dissipative and generative inductor are employed to model: dissipative-dissipative fractional series RLC circuit, consisting of dissipative electric elements, by the governing equation (5); generative-generative circuit, consisting of generative elements, using the governing equation (6); as well as to model dissipative-generative and generative-dissipative circuits, consisting of dissipative capacitor and generative inductor for the former and generative capacitor and dissipative inductor for the latter, by the governing equations (7) and (8).

Constitutive models of dissipative and generative electric elements, expressed in terms of current and voltage, are used in the steady-state regime to define the corresponding impedances and admittances, further to be used in equivalent impedances of the aforementioned RLC circuits. Through the phase angle, the equivalent impedance determines the energy consumption/production properties of the circuit as well as its predominant behavior, see (28) and (34). It is concluded that for each of the circuits capacitive properties prevail for low frequencies, while for the high frequencies inductive properties are dominant, see (39), (44), (49), and (53). As far as the energy consumption/production properties of the fractional RLC circuits are concerned, the dissipative-dissipative circuit consumes energy for all frequencies, see expression (36) and Figure 1, since its constituents are dissipative elements, while all other RLC circuits may both consume and generate energy, depending on the frequency range, see Figures 2, 3, and 4. Since capacitive (inductive) properties are dominant for low (high) frequencies, whether the capacitor (inductor) is dissipative or generative determines the energy consumption/production properties of the circuit itself for low (high) frequencies.

The equivalent impedance of the fractional RLC circuit also determines the explicit form of transfer function modulus and argument, see (55), governing the frequency characteristics. The Bode diagrams, presented in Figures 5, 7, 9, and 11 underline the similarities of the transfer functions corresponding to the fractional RLC circuits with the integer-order transfer functions. Namely, aforementioned figures illustrate that if the transfer function has complex conjugated poles, then the corresponding frequency characteristics of its modulus attains a maximum and then tend to the negative infinity as the frequency tends to infinity, while the occurrence of purely imaginary poles imply that modulus' characteristics has a vertical asymptote. Also, modulus' frequency characteristics illustrate the fact that transfer function has a zero of non-integer order at the origin and indicate that all considered RLC circuits behave as the band-pass filter. Whether the complex conjugated poles of the transfer function have negative or positive real part, determine whether the frequency characteristics of the transfer function argument decreases or increases with the increase of frequency, while if poles are purely imaginary, then argument's characteristics display a sudden drop by π. Predominant character of the fractional RLC circuit, as well as its energy consumption/production properties are discussed by the use of argument's frequency characteristics.

The leading terms in the low and high frequency asymptotics of transfer function modulus and argument are useful in determining model parameters, since for low frequencies, the transfer function modulus is a linear function in $\log\omega$, with the slope α and intercept τ_α in cases of dissipative-dissipative and dissipative-generative RLC circuits, see (60) and (85), while the slope is determined by $1+\mu$ and intercept by τ_μ in cases of generative-generative and generative-dissipative RLC circuits, see (72) and (91). For high frequencies, the transfer function modulus is a linear function in $\log\omega$, with the intercept being τ_L for all fractional RLC circuits, while $\log|\cot\arg\hat{g}(\omega)|$ proves to be a linear function in $\log\omega$, with the slopes $-1+\beta$ and $-\nu$ and intercepts proportional to τ_β and τ_ν, see (66) and (80), in cases of dissipative/generative-dissipative RLC circuit and generative/dissipative-generative RLC circuit, respectively. Figures 6, 8, 10, and 12 vividly illustrate these statements.

Disclosure of potential conflicts of interest - ethical and financial

The authors declare that they have no conflict of interest.

Acknowledgment

This work is supported by the Serbian Ministry of Science, Education and Technological Development under grants 451-03-9/2021-14/200156 (SMC), and 451-03-9/2021-14/200125 (DZ).

References

[1] A. Allagui, A. S. Elwakil, M. E. Fouda, and A. G. Radwan. Capacitive behavior and stored energy in supercapacitors at power line frequencies. *Journal of Power Sources*, 390:142–147, 2018.

[2] A. Allagui, T. J. Freeborn, A. S. Elwakil, M. E. Fouda, B. J. Maundy, A. G. Radwan, Z. Said, and M. A. Abdelkareema. Review of fractional-order electrical characterization of supercapacitors. *Journal of Power Sources*, 400:457–467, 2018.

[3] A. Allagui, D. Zhang, and A. S. Elwakil. Short-term memory in electric double-layer capacitors. *Applied Physics Letters*, 113:253901–1–5, 2018.

[4] M. C. Bošković, T. B. Šekara, B. Lutovac, M. Daković, P. D. Mandić, and M. P. Lazarević. Analysis of electrical circuits including fractional order elements. In *6th Mediterranean Conference on Embedded Computing (MECO)*, Bar, Montenegro, 2017.

[5] A. Buscarino, R. Caponetto, S. Graziani, and E. Murgano. Realization of fractional order circuits by a constant phase element. *European Journal of Control*, 54:64–72, 2020.

[6] R. Caponetto, S. Graziani, and E. Murgano. Realization of a fractional-order RLC circuit via constant phase element. *International Journal of Dynamics and Control*, 9:1589–1599, 2021.

[7] X. Chen, Y. Chen, B. Zhang, and D. Qiu. A modeling and analysis method for fractional-order DC-DC converters. *IEEE Transactions on Power Electronics*, 32:7034–7044, 2017.

[8] A. Dzieliński, G. Sarwas, and D. Sierociuk. Comparison and validation of integer and fractional order ultracapacitor models. *Advances in Difference Equations*, 2011:11:1–15, 2011.

[9] O. Elwy, L. A. Said, A. H. Madian, and A. G. Radwan. All possible topologies of the fractional-order Wien oscillator family using different approximation techniques. *Circuits, Systems, and Signal Processing*, 38:3931–3951, 2019.

[10] M. E. Fouda, A. Allagui, A. S. Elwakil, S. Das, C. Psychalinos, and A. G. Radwan. Nonlinear charge-voltage relationship in constant phase element. *International Journal of Electronics and Communications (AEÜ)*, 117:153104–1–4, 2020.

[11] R. Garrappa, E. Kaslik, and M. Popolizio. Evaluation of fractional integrals and derivatives of elementary functions: Overview and tutorial. *Mathematics*, 7:407–1–21, 2019.

[12] F. Gómez, J. Rosales, and M. Guía. *RLC* electrical circuit of non-integer order. *Central European Journal of Physics*, 11:1361–1365, 2013.

[13] M. Guía, J. Rosales, and F. Gómez. Analysis on the time and frequency domain for the *RC* electric circuit of fractional order. *Central European Journal of Physics*, 11:1366–1371, 2013.

[14] K. Haška, S. M. Cvetićanin, and D. Zorica. Dissipative and generative fractional electric elements in modeling *RC* and *RL* circuits. *Nonlinear Dynamics*, 105:3451–3474, 2021.

[15] K. Haška, D. Zorica, and S. M. Cvetićanin. Fractional *RLC* circuit in transient and steady state regimes. *Communications in Nonlinear Science and Numerical Simulation*, 96:105670–1–17, 2021.

[16] A. Jakubowska and J. Walczak. Analysis of the transient state in a circuit with supercapacitor. *Poznan University of Technology Academic Journals. Electrical Engineering*, 81:71–77, 2015.

[17] A. Jakubowska and J. Walczak. Analysis of the transient state in a series circuit of the class $RL_\beta C_\alpha$. *Circuits, Systems, and Signal Processing*, 35:1831–1853, 2016.

[18] A. Jakubowska-Ciszek and J. Walczak. Analysis of the transient state in a parallel circuit of the class $RL_\beta C_\alpha$. *Applied Mathematics and Computation*, 319:287–300, 2018.

[19] I. S. Jesus and J. A. T. Machado. Development of fractional order capacitors based on electrolyte processes. *Nonlinear Dynamics*, 56:45–55, 2009.

[20] Y. Jiang, B. Zhang, X. Shu, and Z. Wei. Fractional-order autonomous circuits with order larger than one. *Journal of Advanced Research*, 25:217–225, 2020.

[21] D. A. John and K. Biswas. Electrical equivalent circuit modelling of solid state fractional capacitor. *International Journal of Electronics and Communications (AEÜ)*, 78:258–264, 2017.

[22] A. Kartci, A. Agambayev, N. Herencsar, and K. N. Salama. Series-, parallel-, and inter-connection of solid-state arbitrary fractional-order capacitors: Theoretical study and experimental verification. *IEEE Access*, 6:10933–10943, 2018.

[23] A. A. Kilbas, H. M. Srivastava, and J. J. Trujillo. *Theory and Applications of Fractional Differential Equations*. Elsevier B.V., Amsterdam, 2006.

[24] M. S. Krishna, S. Das, K. Biswas, and B. Goswami. Fabrication of a fractional order capacitor with desired specifications: A study on process identification and characterization. *IEEE Transactions on Electron Devices*, 58:4067–4073, 2011.

[25] J. A. T. Machado and A. M. S. F. Galhano. Fractional order inductive phenomena based on the skin effect. *Nonlinear Dynamics*, 68:107–115, 2012.

[26] V. Martynyuk and M. Ortigueira. Fractional model of an electrochemical capacitor. *Signal Processing*, 107:355–360, 2015.

[27] V. Martynyuk, M. Ortigueira, M. Fedula, and O. Savenko. Methodology of electrochemical capacitor quality control with fractional order model. *International Journal of Electronics and Communications (AEÜ)*, 91:118–124, 2018.

[28] D. Mondal and K. Biswas. Packaging of single-component fractional order element. *IEEE Transactions on Device and Materials Reliability*, 13:73–80, 2013.

[29] M. A. Moreles and R. Lainez. Mathematical modelling of fractional order circuit elements and bioimpedance applications. *Communications in Nonlinear Science and Numerical Simulation*, 46:81–88, 2017.

[30] K. Nosrati and M. Shafiee. On the convergence and stability of fractional singular Kalman filter and Riccati equation. *Journal of the Franklin Institute: Engineering and Applied Mathematics*, 357:7188–7210, 2020.

[31] A. V. Oppenheim, A. S. Willsky, and S. H. Nawab. *Signals and systems*. Prentice-Hall signal processing series. Prentice-Hall, New Jersey, 1997.

[32] M. D. Ortigueira and Duarte Valério. *Fractional Signals and Systems*, volume 7 of *Fractional Calculus in Applied Sciences and Engineering*. de Gruyter, Berlin/Boston, 2020.

[33] R. Prasad, K. Kothari, and U. Mehta. Flexible fractional supercapacitor model analyzed in time domain. *IEEE Access*, 7:122626–122633, 2019.

[34] R. Prasad, U. Mehta, and K. Kothari. Various analytical models for supercapacitors: a mathematical study. *Resource-Efficient Technologies*, 1:1–15, 2020.

[35] J. J. Quintana, A. Ramos, and I. Nuez. Modeling of an EDLC with fractional transfer functions using Mittag-Leffler equations. *Mathematical Problems in Engineering*, 2013:807034–1–7, 2013.

[36] A. G. Radwan. Resonance and quality factor of the $RL_\alpha C_\alpha$ fractional circuit. *IEEE Journal on Emerging and Selected Topics in Circuits and Systems*, 3:377–385, 2013.

[37] A. G. Radwan and M. E. Fouda. Optimization of fractional-order *RLC* filters. *Circuits, Systems and Signal Processing*, 32:2097–2118, 2013.

[38] A. G. Radwan and K. N. Salama. Passive and active elements using fractional $L_\beta C_\alpha$ circuit. *IEEE Transactions on Circuits and Systems I: Regular Papers*, 58:2388–2397, 2011.

[39] A. G. Radwan and K. N. Salama. Fractional-order *RC* and *RL* circuits. *Circuits, Systems and Signal Processing*, 31:1901–1915, 2012.

[40] A. G. Radwan, A. M. Soliman, and A. S. Elwakil. Design equations for fractional-order sinusoidal oscillators: Four practical circuit examples. *International Journal of Circuit Theory and Applications*, 36:473–492, 2008.

[41] M. S. Sarafraz and M. S. Tavazoei. Realizability of fractional-order impedances by passive electrical networks composed of a fractional capacitor and *RLC* components. *IEEE Transactions on Circuits and Systems I: Regular Papers*, 62:2829–2835, 2015.

[42] I. Schäfer and K. Krüger. Modelling of coils using fractional derivatives. *Journal of Magnetism and Magnetic Materials*, 307:91–98, 2006.

[43] Z. M. Shah, M. Y. Kathjoo, F. A. Khanday, K. Biswas, and C. Psychalinos. A survey of single and multi-component fractional-order elements (FOEs) and their applications. *Microelectronics Journal*, 84:9–25, 2019.

[44] M. Sowa. A subinterval-based method for circuits with fractional order elements. *Bulletin of the Polish Academy of Sciences Technical Sciences*, 62:449–454, 2014.

[45] M. Sowa. "gcdAlpha" – a semi-analytical method for solving fractional state equations. *Poznan University of Technology Academic Journals. Electrical Engineering*, 96:231–242, 2018.

[46] T. P. Stefański and J. Gulgowski. Electromagnetic-based derivation of fractional-order circuit theory. *Communications in Nonlinear Science and Numerical Simulation*, 79:104897–1–13, 2019.

[47] T. P. Stefański and J. Gulgowski. Signal propagation in electromagnetic media described by fractional-order models. *Communications in Nonlinear Science and Numerical Simulation*, 82:105029–1–16, 2020.

[48] R. Süße, A. Domhardt, and M. Reinhard. Calculation of electrical circuits with fractional characteristics of construction elements. *Forsch Ingenieurwes*, 69:230–235, 2005.

[49] M. S. Tavazoei. Passively realizable approximations of non-realizable fractional order impedance functions. *Journal of the Franklin Institute: Engineering and Applied Mathematics*, 357:7037–7053, 2020.

[50] J. Walczak and A. Jakubowska. Resonance in series fractional order $RL_\beta C_\alpha$ circuit. *Przegląd Elektrotechniczny*, 90:210–213, 2014.

[51] S. Westerlund and L. Ekstam. Capacitor theory. *IEEE Transactions on Dielectrics and Electrical Insulation*, 1:826–839, 1994.

[52] B. Zhang and X. Shu. *Fractional-Order Electrical Circuit Theory*. CPSS Power Electronics Series. Springer, Singapore, 2022.

[53] L. Zhou, Z. Tan, and Q. Zhang. A fractional-order multifunctional n-step honeycomb *RLC* circuit network. *Frontiers of Information Technology and Electronic Engineering*, 18:1186–1196, 2017.